

---

# Generative Modeling Helps Weak Supervision (and Vice Versa)

---

Benedikt Boecking\* Nicholas Roberts† Willie Neiswanger‡  
Stefano Ermon‡ Frederic Sala† Artur Dubrawski\*

\*Carnegie Mellon University †University of Wisconsin ‡Stanford University

## Abstract

Many promising applications of supervised machine learning face hurdles in the acquisition of labeled data in sufficient quantity and quality, creating an expensive bottleneck. To overcome such limitations, techniques that do not depend on ground truth labels have been studied, including weak supervision and generative modeling. While these techniques would seem to be usable in concert, improving one another, how to build an interface between them is not well-understood. In this work, we propose a model fusing programmatic weak supervision and generative adversarial networks and provide theoretical justification motivating this fusion. The proposed approach captures discrete latent variables in the data alongside the weak supervision derived label estimate. Alignment of the two allows for better modeling of sample-dependent accuracies of the weak supervision sources, improving the estimate of unobserved labels. It is the first approach to enable data augmentation through weakly supervised synthetic images and pseudolabels. Additionally, its learned latent variables can be inspected qualitatively. The model outperforms baseline weak supervision label models on a number of multiclass image classification datasets, improves the quality of generated images, and further improves end-model performance through data augmentation with synthetic samples.

## 1 Introduction

How can we get the most out of data when we do not have ground truth labels? Two prominent paradigms operate in this setting. First, programmatic *weak supervision* frameworks use weak sources of training signal to estimate pseudolabels that can be used to train downstream supervised models, without needing access to ground-truth labels [56, 54, 18, 38]. Second, *generative models* enable learning data distributions which can benefit downstream tasks, e.g. via data augmentation or representation learning, in particular when learning latent factors of variation [29, 42, 31]. Intuitively, these two paradigms should complement each other, as each can be thought of as a different approach to extracting structure from unlabeled data. However, to date there is no simple way to combine them.

Fusing generative models with weak supervision holds substantial promise. For example, it should yield large reductions in data acquisition costs for training complex models. Programmatic weak supervision replaces the need for manual annotations by applying so-called labeling functions to all of the unlabeled data, producing weak labels that are combined into a pseudolabel for each unlabeled data point. This leaves the majority of the acquisition budget to be spent on unlabeled data, and here generative modeling can reduce the number of real-world samples that need to be collected. Similarly, the information about the data distribution contained in weak supervision derived

---

\*boecking@cmu.edu, awd@cmu.edu

†nick11roberts@cs.wisc.edu, fredsala@cs.wisc.edu

‡neiswanger@cs.stanford.edu, ermon@cs.stanford.edu

pseudolabels may improve generative models, reducing the need to acquire large volumes of samples to increase the generative performance. Additionally, pseudolabels may allow for class-conditional sample generation without access to ground truth, enabling better, more refined data augmentation.

The main technical challenge is to build an *interface* between the core models used in the two approaches. For example, in the generative adversarial models (GANs) [26] that we focus on in this work, there is at least a generator and a discriminator, and frequently additional auxiliary models, such as those that learn to disentangle latent factors of variation [14]. In weak supervision, the *label model* is the main focus. It is necessary to develop an interface that correctly aligns the structures learned from the unlabeled data by the various components.

We introduce weakly-supervised GAN (WSGAN), a simple but powerful fusion of weak supervision and GANs shown in Fig. 2, and we provide a theoretical justification that motivates the fusion of the techniques and the expected gains. The proposed WSGAN approach is related to the unsupervised InfoGAN [14] generative model, and is also inspired by the encoder-based label model component of a recently-proposed end-to-end weak supervision framework [9]. These techniques expose structure in the data, and our approach ensures alignment between the resulting variables by learning projections between them. Our proposed WSGAN offers a number of benefits, including:

- **Improved weak supervision:** Replacing the conventional label model in weak supervision, we obtain better-quality pseudolabels, yielding consistent improvements in pseudolabel accuracy up to 6% over established programmatic weak supervision techniques such as Snorkel [53].
- **Improved generative modeling:** Weak supervision provides information about unobserved labels which can be used to obtain better disentangled latent variables, thus improving the model’s generative performance. Over 6 datasets, our WSGAN approach improves image generation by an average of 5.8 FID points versus InfoGAN.
- **Data augmentation via synthetic samples:** Our trained WSGAN model can generate synthetic samples and corresponding label estimates for data augmentation (see Fig. 1), enabling further improvements of downstream classifier accuracy of up to 3.9%. The trained WSGAN can produce label estimates even for samples–real or fake–that have no weak supervision signal available.

## 2 Background

As we propose to fuse weak supervision with generative modeling to the benefit of both techniques, we first provide brief background on each of these methods. A broader review of related work is presented in Section 5.

**Weak Supervision** Weak supervision methods using imperfect and partial labels [54, 53, 9], sometimes referred to as programmatic weak supervision, seek to replace hand-labeling for the construction of large training datasets. Instead, users rely on multiple weak sources that, while noisy and inaccurate, can be cheaply acquired and efficiently applied to the entire dataset to provide imperfect, partial labels. Such sources can be heuristics or rules (expressed as small programs), knowledge base lookups, off-the-shelf models, and more.

The technical challenge is to combine the source votes into a high-quality pseudolabel. This requires estimating the errors and dependencies between sources and using them to compute a posterior label distribution. This synthesis step is performed by the *label model*. Prior work has considered various choices for the label model, most of which only take the weak source outputs into account. A review can be found in Zhang et al. [66, 67]. Instead, our label model produces sample dependent accuracy estimates for the weak sources based on the features of the data, similar to Cachay et al. [9].

**Generative Models and GANs** Generative models are used to model and sample from complex distributions. Among the most popular such models are generative adversarial networks (GANs) [26]. GANs consist of a generator and discriminator model that play a minimax game against each



Figure 1: Synthetic images and pseudolabels generated by the proposed WSGAN model for the weakly supervised GT-SRB dataset. WSGAN is able to generate images and estimate their labels, even for images where no weak supervision sources provide information (see end of Section 3.1).

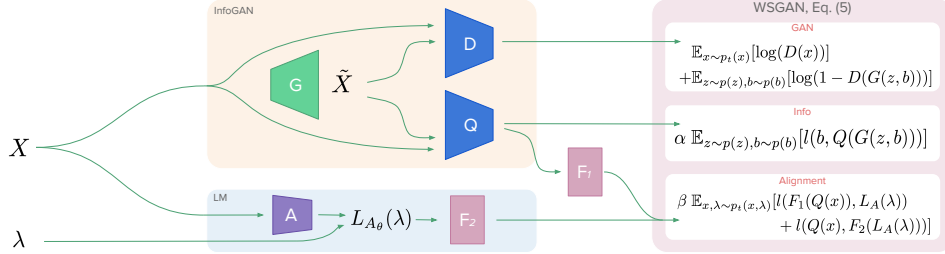


Figure 2: The proposed WSGAN architecture models discrete latent variables in  $X$  via a network  $Q$ , while the generator  $G$  continues to fool the discriminator model  $D$  with generated images  $\tilde{X}$ . Simultaneously, a label model  $L$  receives weights from an accuracy encoder  $A$  to produce an estimate of the unobserved ground truth label of  $X$  based on the observed weak supervision votes  $\lambda$ . The WSGAN model aligns this label estimate with the discrete latent variable learned by  $Q$ .

other. While many sophisticated variations of GANs have been proposed, our approach builds off InfoGAN [14]. InfoGAN adds an auxiliary inference model that helps the generative model learn disentangled representations—a set of latent factors of variation. We hypothesize that connecting these variables to exposed structure in the label model should yield benefits for both weak supervision and generative modeling. Quantitative approaches to measure improved image generation exist, such as the Inception Score (IS) [58] and the Fréchet Inception Distance (FID) [28]. Despite known drawbacks [4, 6], these measures are widely used to compare image quality.

### 3 The WSGAN Model

We first describe our proposed weakly-supervised GAN (WSGAN) model, visualized in Fig. 2, and then provide theoretical justification for the model fusion. We work with  $n$  unlabeled samples  $X \in \mathcal{X} \subseteq \mathbb{R}^d$  drawn from a distribution  $\mathcal{D}_X$ . We want to achieve two goals with the samples  $X$ . First, in generative modeling, we approximate  $\mathcal{D}_X$  with a model that can be used to produce high-fidelity synthetic samples. Second, in supervised learning, we wish to use  $X$  to predict labels  $Y \in \{1, 2, \dots, C\}$ , where  $(X, Y)$  is drawn from a distribution whose marginal distribution is  $\mathcal{D}_X$ . However, in the weak supervision setting, we do not observe  $Y$ . Instead, we observe  $m$  labeling functions that provide imperfect estimates of  $Y$  for a subset of the samples. These labeling functions (LFs), denoted  $\lambda_i$  for  $1 \leq i \leq m$ , vote on a sample  $x$  to produce an estimate  $\lambda_i(x) \in \{0, \dots, C\}$ , where 0 indicates abstain (i.e. no vote). The goal is to combine the  $m$  estimates into a pseudolabel  $\hat{Y}$  that can be used to train a supervised model [54].

While weak supervision and generative modeling function over a number of domains, in this work we focus on images. Image tasks are especially challenging for weak supervision, since constructing LFs is more difficult than for, e.g., text tasks (cf. Section 5).

#### 3.1 Proposed Method

To improve generative performance and the quality of the weak supervision-based pseudolabels, we propose a model that consists of a number of components. Because we wish to ensure our component models benefit each other, our architecture aims for the following characteristics: (I) A generative model component that learns latent factors of variation from data (these could be, for example, discrete structure) and exposes these externally, (II) a weak supervision label model component that uses feature information to make predictions of the unobserved label by aggregating the weak supervision votes, using sample-dependent weights, (III) a set of *interface* models that connect the components. Our design choices are made to satisfy those goals.

**GAN Architecture** We write  $G$  for the generator; its goal is to learn a mapping to the image space based on input consisting of samples  $z$  from a noise distribution  $p_Z(z)$  along with a set of latent factors of variation  $b \sim p(b)$ , following the ideas introduced in Chen et al. [14]. Because we are targeting a classification setting, we restrict ourselves to discrete, disentangled factors of variation. The output of  $G$  are samples  $x$ ; these are consumed by a discriminative model  $D$ , which estimates the probability that a sample came from the training distribution rather than  $G$ .

Furthermore, as in InfoGAN [14], we define an auxiliary model  $Q$  which will learn to map from a sample  $x$  to the discrete latent code  $b$ . This model  $Q$  is used to teach the generator  $G$  disentangled,

discrete representations. First, we write the standard GAN objective as:

$$\min_G \max_D V(D, G) = \mathbb{E}_{x \sim \mathcal{D}_X} [\log(D(x))] + \mathbb{E}_{z \sim p(z), b \sim p(b)} [\log(1 - D(G(z, b)))]. \quad (1)$$

Next, we write the InfoGAN objective as:

$$\min_{G, Q} \max_D IV(D, G, Q) = V(D, G) + \alpha \mathbb{E}_{z \sim p(z), b \sim p(b)} [l(b, Q(G(z, b)))], \quad (2)$$

where  $l$  is an appropriate loss function, such as cross entropy, and  $\alpha$  is a hyperparameter. This approach, presented in Chen et al. [14], aims to maximize the mutual information between generated images and  $b$ , while  $G$  continues to fool the discriminator  $D$ , leading to the discovery of latent factors of variation.

**Weak Supervision Label Model** The purpose of the *label model* is to encode relationships between the LFs  $\lambda_i$  and the unobserved label  $y$ , enabling us to produce an informed estimate of  $y$  based on the LF outputs. The model is usually a factor graph [54, 52, 24, 67] with potentials  $\phi_j(\lambda_j(x), y)$  and  $\phi_{j,k}(\lambda_j(x), \lambda_k(x))$  capturing the degree of agreement between  $\lambda_j$  and  $y$  or correlations between  $\lambda_j$  and  $\lambda_k$ . For example, we set  $\phi_j(\lambda_j, y) \triangleq \mathbb{1}\{\lambda_j = y\}$  as in related work. These potentials  $\phi_j$  are associated with accuracy parameters  $\theta_j$ . Once we obtain estimates of  $\theta_j$ , we can predict  $y$  from the LFs  $\lambda$  using the function  $L_\theta(\lambda) : \{0, 1, \dots, C\}^m \rightarrow [0, 1]^C$ ,

$$L_\theta(\lambda)_k = \frac{\exp(\sum_{j=1}^m \theta_j \phi_j(\lambda_j(x), k))}{\sum_{\tilde{y} \in \mathcal{Y}} \exp(\sum_{j=1}^m \theta_j \phi_j(\lambda_j(x), \tilde{y}))}, \quad \forall k \in \{1, \dots, C\}.$$

This is a softmax over the weighted votes of all LFs, which derives from the factor graph introduced in Ratner et al. [54]. Note that related work only models the LF outputs to learn  $\theta$ , ignoring any additional information in the features  $x$ .

However, the structure in the input data  $x$  is crucial to our fusion. For this reason, we define a modified label model predictor in the spirit of Cachay et al. [9]. It generates *local* accuracy parameters (sample-dependent parameters encoding how accurate each  $\lambda_i$  is estimated to be) via an accuracy parameter encoder  $A(x) : \mathbb{R}^d \rightarrow \mathbb{R}_+^m$ . This variant is given by:

$$L_{A_\theta}(\lambda)_k = \frac{\exp(\sum_{j=1}^m A(x)_j \phi_j(\lambda_j(x), k))}{\sum_{\tilde{y} \in \mathcal{Y}} \exp(\sum_{j=1}^m A(x)_j \phi_j(\lambda_j(x), \tilde{y}))}, \quad \forall k \in \{1, \dots, C\}, \quad (3)$$

a softmax over the LF votes by class, weighted by the accuracy encoder output. Note that, while  $A(x)$  allows for finer-grained adjustments of the label estimate  $\hat{Y}$ , the estimate is still anchored in the votes of LFs which represent strong domain knowledge and are assumed to be better than random.

**Learning the Label Model** The technical challenge of weak supervision is to learn the parameters of the label model (such as  $\theta_j$  above) without observing  $y$ . Existing approaches find parameters under a label model that (i) best explain the LF votes while (ii) satisfying conditionally independent relationships [54, 52, 24]. The features  $x$  are ignored; it is assumed that all information about  $y$  is present in the LF outputs.

We instead promote cooperation between our models by ensuring that *the best label model is the one which agrees with the discrete structure that the GAN can learn, and vice versa*. The intuition for this key notion is that, as each of the generative and label models learn useful information from data, this information can—if aligned correctly—be shared to help teach the other model. To this end, note that in InfoGAN, the model  $Q$  is only applied to generated samples as the sampled variable  $b$  can be observed for generated images, but not for real images. Nonetheless,  $Q$  can be applied to the real-world samples to obtain a prediction of the latent  $b$ . Crucially, in the weak supervision setting we also observe the LF outputs, enabling us derive a label estimate for each real image  $L_{A_\theta}(\lambda) = \hat{Y}$ , which we can use to guide  $Q$ , and vice versa.

**Interface Models and Overall WSGAN Objective** We introduce the following *interface* models to map between the estimates of  $b$  and  $y$ . Let  $F_1 : [0, 1]^C \rightarrow [0, 1]^C$  and  $F_2 : [0, 1]^C \rightarrow [0, 1]^C$ . An effective choice for  $F_1$  and  $F_2$  are linear models with a softmax activation function. To achieve agreement between the latent structure discovered by the GAN’s auxiliary model  $Q$  as well as by the label model  $L_{A_\theta}$  via the LFs, we introduce the following overall objective, ensuring that a mapping exists between the latent structures on the real images in the training data:

$$\min_{G, Q, A, F_1, F_2} \max_D IV(D, G, Q) + \beta \mathbb{E}_{x, \lambda \sim \mathcal{D}_{X, \Lambda}} [l(F_1(Q(x)), L_A(\lambda)) + l(Q(x), F_2(L_A(\lambda)))], \quad (4)$$

where  $\beta$  is a hyperparameter parameter, and  $l$  again denotes an appropriate loss function such as the cross entropy. Pseudocode for the added loss term can be found in Algorithm 1 in the Appendix.

**Improving Alignment** Importantly, initializing the label model  $L_A$  such that it produces equal weights for all LFs results in a strong baseline estimate of  $\hat{Y}$ , as LFs are built to be better than random. Initializing  $L_{A_\theta}$  in this way, it can act as a teacher in the beginning and guide  $Q$  towards the discrete structure encoded in the LFs. To reinforce this behavior and to stabilize learning, we find that adding a decaying penalty term that encourages equal label model weights in early epochs—while not necessary to achieve good performance—almost always improves latent label estimates further. Let  $i \geq 0$  denote the current epoch. We propose to add the following linearly decaying penalty term for an encoder  $A$  that uses a sigmoid activation function:  $C/(i \times \gamma + 1) \|A(x) - \bar{1} \times 0.5\|_2^2$ , where  $\gamma$  is a decay parameter. In our experiments we set  $\gamma = 1.5$ . Regarding parameters to be learned, note that  $D, Q, A$  all encode images. As common in related GAN work, we let  $D, Q$  and  $A$  share convolutional layers and define distinct prediction heads for each. For  $L_A$  we detach the output of the convolutional layers from the computation graph before passing it to a small multilayer perceptron (MLP) followed by a sigmoid activation function. Thus, the WSGAN method only adds a small number of additional parameters compared to a basic GAN or InfoGAN.

**Augmenting the Weak Supervision Pipeline with Synthetic Data** Given a WSGAN model trained according to Eq. 4, we can generate images via  $G$  to obtain unlabeled synthetic samples  $\tilde{x}$ . To obtain pseudolabels for these images we have at least one and sometimes two options. When LFs can be applied to synthetic images, we can obtain their votes  $\lambda(\tilde{x}) = \tilde{\lambda}$  and apply our WSGAN label model  $L_A(\tilde{\lambda})$ . However, in many practical applications of weak supervision, some LFs are not applied to images directly, but rather to metadata or an auxiliary modality such as text (cf. Section 5). With WSGAN, we can obtain pseudolabels via  $\hat{y} = F_1(Q(\tilde{x}))$  for samples that have no LF votes, using the trained WSGAN components  $Q$  and  $F_1$ , in essence transferring knowledge from  $Q$  to the end model. Note that the quality of these synthetic pseudolabels hinges on the performance of  $Q$ , which can conceivably improve with the supply of weakly supervised as well as entirely unlabeled data.

### 3.2 Theoretical Justification

In this section, we provide theoretical results that suggest that there is a provable benefit to combining weak supervision and generative modeling. In particular, we provide two theoretical claims justifying why *weak supervision should help generative modeling (and vice versa)*: (1) generative models help weak supervision via a generalization bound on downstream classification and (2) weak supervision improves a multiplicative approximation bound on the loss for a conditional GAN trained using noisy labels—namely the Robust Conditional GAN (RCGAN) [61]. Formal statements and proofs of these claims can be found in Appendix F.

**Claim (1)** Assume that we have  $n_1$  unlabeled real examples where our label model fails to produce labels, i.e. all LFs abstain on these  $n_1$  points. This is a typical issue in weak supervision. We then sample enough synthetic examples from our generative model such that we obtain  $n_2$  synthetic examples for which our label model *does* produce labels; this enables training of a downstream classifier on synthetic examples alone with the following generalization bound:

$$\sup_{f \in \mathcal{F}} |\hat{\mathbb{R}}_{\mathcal{D}}(f) - \mathbb{R}_{\mathcal{D}}(f)| \leq 2\mathfrak{R} + \sqrt{\frac{\log(1/\delta)}{2n_2}} + B_\ell G^{\frac{1}{2}} + B_\ell \sqrt{2} \exp(-m\alpha^2).$$

Where  $\mathfrak{R}$  is the Rademacher complexity of the function class. The first two terms are standard. The third term is the penalty due to generative model usage; any generative model estimation result for total variation distance can be plugged in. For example, for estimating a mixture of Gaussians,  $G = (4c_G k d^2 / n_1)^{1/2}$  which depends on the number of mixture components  $k$  and dimension  $d$ . The last term is the penalty from weak supervision with  $m$  LFs whose accuracy is  $\alpha$  better than chance; this implies that generated samples can help weak supervision generalize when true samples cannot.

**Claim (2)** Let  $d_{\mathcal{F}}(\tilde{P}_{\text{MV}}, \tilde{Q}_{\text{MV}})$  be the RCGAN loss with noisy labels generated by majority vote and let  $\epsilon_\lambda$  be the mean error of each LF. Using majority vote with  $m \geq 0.5 \log(1/\epsilon_\lambda) / (\frac{1}{2} - \epsilon_\lambda)^2$  LFs, we obtain an exponentially tighter multiplicative bound on the noiseless RCGAN loss:

$$\begin{aligned} d_{\mathcal{F}}(\tilde{P}_{\text{MV}}, \tilde{Q}_{\text{MV}}) &\leq d_{\mathcal{F}}(P, Q) \leq \left(1 - 2 \exp\left(-2m \left(\frac{1}{2} - \epsilon_\lambda\right)^2\right)\right)^{-1} d_{\mathcal{F}}(\tilde{P}_{\text{MV}}, \tilde{Q}_{\text{MV}}) \\ &\leq (1 - 2\epsilon_\lambda)^{-1} d_{\mathcal{F}}(\tilde{P}_{\text{MV}}, \tilde{Q}_{\text{MV}}). \end{aligned}$$

Table 1: Datasets and labeling function (LF) characteristics used to evaluate the proposed WSGAN. Acc denotes accuracy, and Coverage denotes the proportion of samples where the LF does not abstain.

Dataset	#Classes	#LFs	#Samples	Mean LF Acc	Min LF Acc	Max LF Acc	Mean Coverage	LF Type
AwA2 -A	10	29	6726	0.504	0.053	0.850	0.104	Attribute heuristics
AwA2 -B	10	32	6726	0.548	0.116	0.783	0.131	Attribute heuristics
DomainNet	10	4	6369	0.493	0.416	0.684	1.000	Domain transfer
MNIST	10	29	30000	0.791	0.564	0.931	0.047	SSL, finetuning
FashionMNIST	10	23	30000	0.773	0.542	0.949	0.047	SSL, finetuning
GTSRB	43	100	22640	0.837	0.609	0.949	0.007	SSL, finetuning
CIFAR10-A	10	20	30000	0.773	0.624	0.896	0.061	Synthetic
CIFAR10-B	10	20	30000	0.736	0.531	0.912	0.042	SSL, finetuning

This means that weak supervision can help an RCGAN more-accurately learn the true joint distribution, even when the true labels are unobserved.

## 4 Experiments

Our experiments on multiple image datasets show that the proposed WSGAN approach is able to take advantage of the discrete latent structure it discovers in the images, leading to better performance compared to label models of prior work. Our results also indicate that weak supervision as used by WSGAN can improve image generation performance, as well as the quality of the auxiliary model which learns disentangled discrete structure. We will first describe the experimental setup and then discuss the results. Additional experiments, baselines (e.g. comparing against naive combinations of weak supervision and generative modeling), and metrics can be found in Appendix C,D, and E. Code for the WSGAN model is available at <https://github.com/anonymous> is supplied in the Supplemental material.

### 4.1 Setup

**Datasets** Table 1 shows key characteristics of the datasets used in our experiments, including information about the different LF sets. We conduct experiments with the 3-channel color image datasets Animals with Attributes 2 (AwA2) [43], DomainNet [50], the German Traffic Sign Recognition Benchmark (GTSRB) [60], and CIFAR10 [37] as well as with the 1-channel gray-scale MNIST [39] and FashionMNIST [64] datasets. See Appendix B for more dataset details.

We use a variety of weak supervision sources for these datasets and provide a more detailed description in Appendix B.1:

- *Domain transfer*: classifiers are trained on images in source domains (e.g. sketches, paintings), and the trained classifiers are then applied to images in a target domain (e.g. real images) to obtain weak labels. This LF type is used in our DomainNet experiments, following [43].
- *Attribute heuristics*: are used in our AwA2 experiments. Attribute classifiers are trained on a number of seen classes of animals. Given these weak attribute predictions, we use the known attribute relations and a small amount of validation data to train shallow decision trees to produce weak labels for a set of unseen classes of animals.
- *SSL-based*: to produce weak labels based on representations learned via self-supervised learning (SSL), we fine-tune shallow multilayer perceptron classifiers on small held-out data using SSL features. The base representations are learned on unsupervised ImageNET with SimCLR [12].
- *Synthetic*: these simulated LFs, used in some of our CIFAR10 experiments, are unipolar LFs based on the corrupted true class label. To this end, random errors are introduced to the class label to achieve a sampled target accuracy and propensity.

**Models** We evaluate the following versions of the proposed WSGAN model:

- WSGAN-Encoder: our proposed model, weighing LF votes of each sample by using the output of an *accuracy parameter encoder*  $A$  that takes in the image associated with a sample and outputs a weight vector to the label model.
- WSGAN-Vector: a baseline derived from the proposed model, using a simple parameter vector to weigh LF votes in place of the encoder  $A$ .

For the implementation of InfoGAN and the GAN component of WSGAN we use a simple DC-GAN [51] base encoder and decoder architecture. All networks are trained from scratch and we use the same hyperparameter settings in all experiments. We provide further implementation details and parameter settings in Appendix A.

Table 2: Average posterior accuracy of various label models on training samples with at least one LF vote. We highlight the best result in **blue** and the second best result in **bold**.

Dataset	MV	DawidSkene	MeTaL	FS	Snorkel	WSGAN-Vector	WSGAN-Encoder
AwA2 - A	0.631	0.607	0.632	0.615	0.641	<b>0.647</b>	<b>0.681</b>
AwA2 - B	0.623	0.548	0.582	0.602	0.605	<b>0.645</b>	<b>0.699</b>
DomainNet	0.614	<b>0.658</b>	0.487	0.635	0.499	<b>0.661</b>	0.643
MNIST	0.775	0.729	0.766	0.773	0.766	<b>0.782</b>	<b>0.813</b>
FashionMNIST	<b>0.735</b>	0.717	0.730	0.734	0.729	<b>0.737</b>	<b>0.744</b>
GTSRB	<b>0.816</b>	0.619	<b>0.815</b>	0.671	<b>0.814</b>	<b>0.815</b>	<b>0.823</b>
CIFAR10-A	0.827	<b>0.850</b>	0.806	0.800	0.807	<b>0.850</b>	<b>0.874</b>
CIFAR10-B	0.716	0.677	0.708	0.708	0.707	<b>0.725</b>	<b>0.731</b>

We provide performance comparisons to the following related label model approaches:<sup>4</sup>

- Snorkel [54, 53]: a probabilistic graphical model that estimates LF parameters by maximizing the marginal likelihood using observed LFs.
- Dawid-Skene [17]: a model motivated by the crowdsourcing setting. The model, fit using expectation maximization, assumes that error statistics of sources are the same across classes and that errors are equiprobable independent of the true class.
- Snorkel MeTaL [52]: a Markov random field (MRF) model similar to Snorkel which uses a technique to complete the inverse covariance matrix of the MRF during model fitting, and also allows for modeling multi-task weak supervision.
- FlyingSquid (FS) [24]: based on a label model similar to Snorkel, FS provides a closed form solution by augmenting it to set up a binary Ising model, enabling scalable model fitting.
- Majority Vote (MV): A standard scheme that uses the most popular LF output as the estimate of the true label.

**Evaluation Metrics** Label model performance is compared based on the pseudolabel accuracy the models achieve on the training data (weighted F1 and mean Average Precision are provided in Appendix E). To compare the quality of generated images, we use the Fréchet Inception Distance (FID) on color images, which has been shown to be consistent with human judgments and to be more robust than related measures [28]. While FID is known to be biased as a function of the generator and number of generated samples [16], the relative ordering in this paper is informative as we use the same generator and training samples for WSGAN and InfoGAN. To show the improvement in alignment of the auxiliary model  $Q$ 's predictions of the discrete latent code  $b$  with the latent labels  $y$ , we track the Adjusted Rand Index (ARI) between the two during training.

## 4.2 Results

We first discuss results comparing label model and image generation performance, before presenting the use of WSGAN for augmentation of the downstream classifier with synthetic samples. We repeat each experiment at least three times and average the results in our tables.

### 4.2.1 Label Model and Image Generation

**Label Model Performance** Table 2 shows a comparison of label model performance based on the accuracy of the posterior on the training data, without the use of any labeled data or validation sets. WSGAN-encoder largely outperforms alternative label models, while the simpler WSGAN-vector model performs competitively as well. These results hold according to additional metrics provided in Appendix C. A limited computation budget restricted us from conducting a large number of runs for all datasets and model combinations. However, results with standard deviations over 5 random runs are provided in the Appendix in Table 10, indicating that many differences are significant.

**Discrete Latent Code Comparison** Figure 3 shows the evolving ARI between the ground truth and the auxiliary model  $Q$ 's prediction of the latent code on real data during model training. The figures show a large improvement in  $Q$ 's ability discover the unobserved class label structure when comparing WSGAN to InfoGAN, which is expected as WSGAN can take advantage of the weak signals encoded in LFs, while InfoGAN is completely unsupervised.

<sup>4</sup>Implementations available via WRENCH [66]

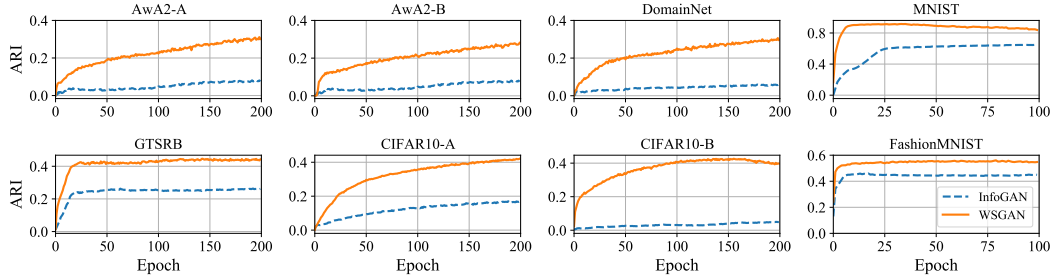


Figure 3: Adjusted Rand Index between the unobserved class label  $y$  and the discrete code prediction by the auxiliary model  $Q(x)$  on real image  $x$ , during training. Weak supervision allows WSGAN to better uncover the latent class structure compared to an unsupervised InfoGAN.

**Image Generation Performance** Table 3 compares FID of generated color images, suggesting that WSGAN models do take advantage of the weak supervision signal to improve  $Q$ , thereby improving the quality of generated images compared to an InfoGAN of the same architecture.

#### 4.2.2 Synthetic Data Augmentation

We record the change in test accuracy for a ResNet-18 [27] end model when adding 1,000 synthetic WSGAN-encoder images  $\tilde{x}$  to augment each dataset. While the increases are modest, performance did not decrease, and the process does not require additional human labeling or data collection efforts.

#### Synthetic Images with Labeling Function Votes

We apply LFs to the generated images  $\tilde{x}$  to obtain LF votes  $\lambda(\tilde{x})$ . We obtain pseudolabels via the WSGAN label model  $L_{A(\tilde{x})}(\lambda(\tilde{x}))$ . The last column in Table 4 displays improvements in test accuracy up to 3.9%.

#### Synthetic Images with Synthetic Pseudolabels

Without access to LF votes on fake images, we create synthetic pseudolabels  $F_1(Q(\tilde{x}))$ . The second column of Table 4 shows the increase in test accuracy, indicating that a modest increase of up to 2.4% was achieved. We do not observe larger increases in accuracy by adding more generated images. Figure 1 shows a small number of generated images along with synthetic pseudolabel estimates. While  $F_1(Q(x))$  could conceivably be used as a downstream classifier, the choices of architecture are constrained as it shares convolutional layers with  $D$ .

#### Synthetic Data Quality Checks

In addition to visually inspecting some generated samples and checking if conditionally generated samples reflect the target labels, we recommend checking the class balance in the pseudolabels of synthetic images before adding them to a downstream training set, as mode collapse in a trained GAN can potentially be diagnosed this way. We were able to automatically discard some low quality sets of generated images this way.

## 5 Related Work

We review relevant work in weak supervision, generative modeling, and data augmentation via GANs.

**Programmatic Weak Supervision** Data programming (DP) [54] is a popular weak supervision framework in which subject matter experts programmatically label data through multiple noisy

Table 3: Color image generation quality measured by average Fréchet Inception Distance (FID). The best scores for each dataset are highlighted in blue.

Dataset	InfoGAN	WSGAN-V	WSGAN-E
AwA2 - A	41.62	36.74	<b>34.71</b>
AwA2 - B	41.62	36.79	<b>34.52</b>
DomainNet	53.98	50.16	<b>44.35</b>
GTSRB	<b>69.67</b>	75.27	73.96
CIFAR10-A	28.93	25.70	<b>22.71</b>
CIFAR10-B	33.50	26.17	<b>24.41</b>

Table 4: Increase in test accuracy when augmenting downstream classifier training with 1,000 synthetic images and corresponding pseudolabels (PLs). Synthetic PLs are obtained via  $F_1(Q(\tilde{x}))$ , LF PLs via  $L_{A(\tilde{x})}(\lambda(\tilde{x}))$ .

Dataset	Synthetic PLs	LF PLs
AwA2 - A	0.88%	0.79%
AwA2 - B	2.40%	3.90%
DomainNet	2.31%	1.50%
MNIST	1.60%	1.71%
FashionMNIST	0.29%	0.34%
GTSRB	0.40%	0.02%
CIFAR10-A	0.04%	-
CIFAR10-B	0.30%	-

sources of labels known as labeling functions (LFs). These LFs capture partial knowledge about an unobserved ground truth variable at better than random accuracy. In this paradigm, LF votes are combined to derive an estimate of the unobserved ground truth, which is then used to train an end model using a noise-aware loss function. DP has been successfully applied to various domains including medicine [23, 21, 22] and industry applications [55, 3].

Many works offer data programming label models with improved properties, e.g., extensions to multitask models [52], better computational efficiency [24], exploiting small amounts of labels as in semi-supervised learning [11, 43, 44], end-to-end training [9], interactive learning [5], or extensions to structured prediction settings [59]. See [67] for a detailed survey.

**Programmatic Weak Supervision and Images** Our main focus is on applications of weak supervision to image data. On images, imperfect labels are often obtained from domain specific primitives and rules [62, 23], rules defined on top of annotations by surrogate models [62, 13, 30], and rules defined on meta-data [40, 15, 33, 19, 5] or a second paired modality such as text [34, 63, 32, 57, 21, 22].

**Generative Models and Disentangled Representations** Among the numerous existing approaches to generative modeling, in this work we focus on generative adversarial networks (GANs) [26]. We are particularly interested in work that aims to learn disentangled representations [14, 41] that can align with class variables of interest. Chen et al. [14] introduce InfoGAN, which learns interpretable latent codes. This is achieved by maximizing the mutual information between a fixed small subset of the GAN’s input variables and the generated observations. Gabbay and Hoshen [25] present a unified formulation for class and content disentanglement as well as a new approach for class-supervised content disentanglement. Nie et al. [47] study semi-supervised high-resolution disentanglement learning for the state-of-the-art StyleGAN architecture. A potential downside to modeling latent factors in generative models is a decrease in image quality of generated samples that has been noted when disentanglement terms are added [8, 36].

Prior work has studied how to integrate additional information into GAN training, in particular ground truth class labels [45, 48, 7, 61]. However, in the programmatic weak supervision setting, having multiple noisy sources of imperfect labels that include abstains present large hurdles to similar conditional modeling. Some prior work uses other weak formats of supervision to aid specific aspects of generative modeling. For example, Chen and Batmanghelich [10] propose learning disentangled representation using user-provided ground-truth pairs. Yet, prior work does not fuse programmatic weak supervision frameworks and generative models, and so are limited to one-off techniques to solely improve generative models.

**Using GANs for Data Augmentation** An exciting application of GANs is to generate additional samples for supervised model training. The challenge is to produce sufficiently high-quality samples. For example, Abbas et al. [1] use a conditional GAN to generate synthetic images of tomato plant leaves for a disease detection task. GANs for data augmentation are also popular in medical imaging [65, 46, 31]. For example, Hu et al. [31] use an InfoGAN-like model to learn cell-level representations in histopathology, Motamed et al. [46] augment radiology data, and Pascual et al. [49] generate synthetic epileptic brain activities.

## 6 Conclusion

We studied the question of how to build an interface between two powerful techniques that operate in the absence of labeled data: generative modeling and programmatic weak supervision. Our fusion of the two, a weakly supervised GAN (WSGAN), defines an interface that aligns structures discovered in its constituent models. This leads to three improvements: first, better quality pseudolabels compared to weak supervision alone, boosting downstream performance. Second, improvement in the quality of the generative model samples. Third, the enablement of data augmentation using such samples, further improving downstream model performance without additional burden on users.

Our proposed approach leads to several exciting directions for future work. We plan to extend the generative model component in the fused model to progressively grown GANs [35] to handle larger and higher fidelity images. We are also interested in other modalities, exploiting for instance generative models for graphs and time series. Finally, motivated by the performance of WSGAN, we seek to extend the underlying notion of interfaces between models to a variety of other pairs of models. Limitations of the proposed approach include common GAN restrictions such as the types of data that can be modeled and the number of unlabeled samples required to fit distributions, and also known difficulties of acquiring weak supervision sources of sufficient quality for image data.

## Acknowledgments and Disclosure of Funding

This work was partially supported by a Space Technology Research Institutes grant from NASA’s Space Technology Research Grants Program and the Defense Advanced Research Projects Agency’s award FA8750-17-2-0130. This work was also supported in part by NSF (#1651565, #CCF2106707) and ARO (W911NF2110125), and the Wisconsin Alumni Research Foundation (WARF).

## References

- [1] Amreen Abbas, Sweta Jain, Mahesh Gour, and Swetha Vankudothu. Tomato plant disease detection using transfer learning with c-gan synthetic images. *Computers and Electronics in Agriculture*, 187:106279, 2021.
- [2] Hassan Ashtiani, Shai Ben-David, Nicholas JA Harvey, Christopher Liaw, Abbas Mehrabian, and Yaniv Plan. Nearly tight sample complexity bounds for learning mixtures of gaussians via sample compression schemes. In *Proceedings of the 32nd International Conference on Neural Information Processing Systems*, pages 3416–3425, 2018.
- [3] Stephen H Bach, Daniel Rodriguez, Yintao Liu, Chong Luo, Haidong Shao, Cassandra Xia, Souvik Sen, Alex Ratner, Braden Hancock, Houman Alborzi, et al. Snorkel drybell: A case study in deploying weak supervision at industrial scale. In *Proceedings of the 2019 International Conference on Management of Data*, pages 362–375, 2019.
- [4] Shane Barratt and Rishi Sharma. A note on the inception score. *arXiv preprint arXiv:1801.01973*, 2018.
- [5] Benedikt Boecking, Willie Neiswanger, Eric Xing, and Artur Dubrawski. Interactive weak supervision: Learning useful heuristics for data labeling. In *International Conference on Learning Representations*, 2021.
- [6] Ali Borji. Pros and cons of gan evaluation measures. *Computer Vision and Image Understanding*, 179:41–65, 2019.
- [7] Andrew Brock, Jeff Donahue, and Karen Simonyan. Large scale GAN training for high fidelity natural image synthesis. In *International Conference on Learning Representations*, 2019.
- [8] Christopher P Burgess, Irina Higgins, Arka Pal, Loic Matthey, Nick Watters, Guillaume Desjardins, and Alexander Lerchner. Understanding disentangling in  $\beta$ -vae. *arXiv preprint arXiv:1804.03599*, 2018.
- [9] Salva Rühling Cachay, Benedikt Boecking, and Artur Dubrawski. End-to-end weak supervision. *Thirty-fifth Conference on Neural Information Processing Systems (NeurIPS)*, 2021.
- [10] Junxiang Chen and Kayhan Batmanghelich. Weakly supervised disentanglement by pairwise similarities. In *Proceedings of the AAAI Conference on Artificial Intelligence*, volume 34, pages 3495–3502, 2020.
- [11] Mayee Chen, Benjamin Cohen-Wang, Stephen Mussmann, Frederic Sala, and Christopher Ré. Comparing the value of labeled and unlabeled data in method-of-moments latent variable estimation. In *International Conference on Artificial Intelligence and Statistics*, pages 3286–3294. PMLR, 2021.
- [12] Ting Chen, Simon Kornblith, Mohammad Norouzi, and Geoffrey Hinton. A simple framework for contrastive learning of visual representations. In *International conference on machine learning*, pages 1597–1607. PMLR, 2020.
- [13] Vincent Chen, Sen Wu, Alexander J Ratner, Jen Weng, and Christopher Ré. Slice-based learning: A programming model for residual learning in critical data slices. In *Advances in Neural Information Processing Systems*, pages 9392–9402, 2019.
- [14] Xi Chen, Yan Duan, Rein Houthoofd, John Schulman, Ilya Sutskever, and Pieter Abbeel. Infogan: interpretable representation learning by information maximizing generative adversarial nets. In *Neural Information Processing Systems (NIPS)*, 2016.

- [15] Xinlei Chen and Abhinav Gupta. Webly supervised learning of convolutional networks. In *Proceedings of the IEEE International Conference on Computer Vision*, pages 1431–1439, 2015.
- [16] Min Jin Chong and David Forsyth. Effectively unbiased fid and inception score and where to find them. In *Proceedings of the IEEE/CVF conference on computer vision and pattern recognition*, pages 6070–6079, 2020.
- [17] Alexander Philip Dawid and Allan M Skene. Maximum likelihood estimation of observer error-rates using the em algorithm. *Journal of the Royal Statistical Society: Series C (Applied Statistics)*, 28(1):20–28, 1979.
- [18] Mostafa Dehghani, Hamed Zamani, Aliaksei Severyn, Jaap Kamps, and W. Bruce Croft. Neural ranking models with weak supervision. In *Proceedings of the 40th International ACM SIGIR Conference on Research and Development in Information Retrieval*, page 65–74. Association for Computing Machinery, 2017.
- [19] Emily Denton, Jason Weston, Manohar Paluri, Lubomir Bourdev, and Rob Fergus. User conditional hashtag prediction for images. In *Proceedings of the 21th ACM SIGKDD international conference on knowledge discovery and data mining*, pages 1731–1740, 2015.
- [20] John Duchi. Lecture notes for statistics 311/electrical engineering 377. URL: [https://stanford.edu/class/stats311/Lectures/full\\_notes.pdf](https://stanford.edu/class/stats311/Lectures/full_notes.pdf). Last visited on, 2:23, 2016.
- [21] Jared A. Dunnmon, Alexander J. Ratner, Khaled Saab, Nishith Khandwala, Matthew Markert, Hersh Sagreiya, Roger Goldman, Christopher Lee-Messer, Matthew P. Lungren, Daniel L. Rubin, and Christopher Re. Cross-modal data programming enables rapid medical machine learning. *Patterns*, 1(2):100019, 2020.
- [22] Sabri Eyuboglu, Geoffrey Angus, Bhavik N Patel, Anuj Pareek, Guido Davidzon, Jin Long, Jared Dunnmon, and Matthew P Lungren. Multi-task weak supervision enables anatomically-resolved abnormality detection in whole-body fdg-pet/ct. *Nature communications*, 12(1):1–15, 2021.
- [23] Jason A Fries, Paroma Varma, Vincent S Chen, Ke Xiao, Heliodoro Tejeda, Priyanka Saha, Jared Dunnmon, Henry Chubb, Shiraz Maskatia, Madalina Fiterau, et al. Weakly supervised classification of aortic valve malformations using unlabeled cardiac mri sequences. *Nature Communications*, 10(1):1–10, 2019.
- [24] Daniel Y. Fu, Mayee F. Chen, Frederic Sala, Sarah M. Hooper, Kayvon Fatahalian, and Christopher Ré. Fast and three-rious: Speeding up weak supervision with triplet methods, 2020.
- [25] Aviv Gabbay and Yedid Hoshen. Demystifying inter-class disentanglement. In *International Conference on Learning Representations*, 2020.
- [26] Ian J. Goodfellow, Jean Pouget-Abadie, Mehdi Mirza, Bing Xu, David Warde-Farley, Sherjil Ozair, Aaron Courville, and Yoshua Bengio. Generative adversarial nets. In *Proceedings of the 27th International Conference on Neural Information Processing Systems - Volume 2, NIPS' 14*, page 2672–2680, 2014.
- [27] Kaiming He, Xiangyu Zhang, Shaoqing Ren, and Jian Sun. Deep residual learning for image recognition. In *Proceedings of the IEEE Conference on Computer Vision and Pattern Recognition*, pages 770–778, 2016.
- [28] Martin Heusel, Hubert Ramsauer, Thomas Unterthiner, Bernhard Nessler, and Sepp Hochreiter. Gans trained by a two time-scale update rule converge to a local nash equilibrium. *Advances in neural information processing systems*, 30, 2017.
- [29] Irina Higgins, David Amos, David Pfau, Sebastien Racaniere, Loic Matthey, Danilo Rezende, and Alexander Lerchner. Towards a definition of disentangled representations. *arXiv preprint arXiv:1812.02230*, 2018.

- [30] Sarah Hooper, Michael Wornow, Ying Hang Seah, Peter Kellman, Hui Xue, Frederic Sala, Curtis Langlotz, and Christopher Ré. Cut out the annotator, keep the cutout: better segmentation with weak supervision. *International Conference on Learning Representations (ICLR)*, 2021.
- [31] B. Hu, Y. Tang, E. I. C. Chang, Y. Fan, M. Lai, and Y. Xu. Unsupervised learning for cell-level visual representation in histopathology images with generative adversarial networks. *IEEE Journal of Biomedical and Health Informatics*, 23(3):1316–1328, 2019. doi: 10.1109/JBHI.2018.2852639.
- [32] Jeremy Irvin, Pranav Rajpurkar, Michael Ko, Yifan Yu, Silviana Ciurea-Ilcus, Chris Chute, Henrik Marklund, Behzad Haghgoo, Robyn Ball, Katie Shpanskaya, et al. Chexpert: A large chest radiograph dataset with uncertainty labels and expert comparison. In *Proceedings of the AAAI conference on artificial intelligence*, volume 33, pages 590–597, 2019.
- [33] Hamid Izadinia, Bryan C Russell, Ali Farhadi, Matthew D Hoffman, and Aaron Hertzmann. Deep classifiers from image tags in the wild. In *Proceedings of the 2015 Workshop on Community-Organized Multimodal Mining: Opportunities for Novel Solutions*, pages 13–18, 2015.
- [34] Armand Joulin, Laurens Van Der Maaten, Allan Jabri, and Nicolas Vasilache. Learning visual features from large weakly supervised data. In *European Conference on Computer Vision*, pages 67–84. Springer, 2016.
- [35] Tero Karras, Timo Aila, Samuli Laine, and Jaakko Lehtinen. Progressive growing of gans for improved quality, stability, and variation. In *International Conference on Learning Representations*, 2018.
- [36] Valentin Khruikov, Leyla Mirvakhabova, Ivan Oseledets, and Artem Babenko. Disentangled representations from non-disentangled models. *arXiv preprint arXiv:2102.06204*, 2021.
- [37] Alex Krizhevsky. Learning multiple layers of features from tiny images. 2009.
- [38] Hunter Lang and Hoifung Poon. Self-supervised self-supervision by combining deep learning and probabilistic logic. In *In Proceedings of the Thirty Fifth Annual Meeting of the Association for the Advancement of Artificial Intelligence (AAAI)*, 2021.
- [39] Yann LeCun, Léon Bottou, Yoshua Bengio, and Patrick Haffner. Gradient-based learning applied to document recognition. *Proceedings of the IEEE*, 86(11):2278–2324, 1998.
- [40] Li-Jia Li and Li Fei-Fei. Optimol: automatic online picture collection via incremental model learning. *International journal of computer vision*, 88(2):147–168, 2010.
- [41] Zinan Lin, Kiran Thekumparampil, Giulia Fanti, and Sewoong Oh. Infogan-cr and modelcentrality: Self-supervised model training and selection for disentangling gans. In *International Conference on Machine Learning*, pages 6127–6139. PMLR, 2020.
- [42] Francesco Locatello, Gabriele Abbati, Tom Rainforth, Stefan Bauer, Bernhard Schölkopf, and Olivier Bachem. On the fairness of disentangled representations. *arXiv preprint arXiv:1905.13662*, 2019.
- [43] Alessio Mazzetto, Cyrus Cousins, Dylan Sam, Stephen H Bach, and Eli Upfal. Adversarial multi class learning under weak supervision with performance guarantees. In *International Conference on Machine Learning*, pages 7534–7543. PMLR, 2021.
- [44] Alessio Mazzetto, Dylan Sam, Andrew Park, Eli Upfal, and Stephen Bach. Semi-supervised aggregation of dependent weak supervision sources with performance guarantees. In *International Conference on Artificial Intelligence and Statistics*, pages 3196–3204. PMLR, 2021.
- [45] Mehdi Mirza and Simon Osindero. Conditional generative adversarial nets. *arXiv preprint arXiv:1411.1784*, 2014.
- [46] Saman Motamed, Patrik Rogalla, and Farzad Khalvati. Data augmentation using generative adversarial networks (gans) for gan-based detection of pneumonia and covid-19 in chest x-ray images. *Informatics in Medicine Unlocked*, 27:100779, 2021. ISSN 2352-9148. doi: <https://doi.org/10.1016/j.imu.2021.100779>.

- [47] Weili Nie, Tero Karras, Animesh Garg, Shoubhik Debnath, Anjul Patney, Ankit Patel, and Animashree Anandkumar. Semi-supervised stylegan for disentanglement learning. In *International Conference on Machine Learning*, pages 7360–7369. PMLR, 2020.
- [48] Augustus Odena, Christopher Olah, and Jonathon Shlens. Conditional image synthesis with auxiliary classifier gans. In *International conference on machine learning*, pages 2642–2651. PMLR, 2017.
- [49] Damián Pascual, Amir Aminifar, David Atienza, Philippe Ryvlin, and Roger Wattenhofer. Synthetic epileptic brain activities using gans. *Machine Learning for Health (ML4H) at NeurIPS*, 2019.
- [50] Xingchao Peng, Qinxun Bai, Xide Xia, Zijun Huang, Kate Saenko, and Bo Wang. Moment matching for multi-source domain adaptation. In *Proceedings of the IEEE/CVF International Conference on Computer Vision*, pages 1406–1415, 2019.
- [51] Alec Radford, Luke Metz, and Soumith Chintala. Unsupervised representation learning with deep convolutional generative adversarial networks. *arXiv preprint arXiv:1511.06434*, 2015.
- [52] Alexander Ratner, Braden Hancock, Jared Dunnmon, Frederic Sala, Shreyash Pandey, and Christopher Ré. Training complex models with multi-task weak supervision. In *Proceedings of the AAAI Conference on Artificial Intelligence*, volume 33, pages 4763–4771, 2019.
- [53] Alexander Ratner, Stephen H Bach, Henry Ehrenberg, Jason Fries, Sen Wu, and Christopher Ré. Snorkel: Rapid training data creation with weak supervision. *The VLDB Journal*, 29(2): 709–730, 2020.
- [54] Alexander J Ratner, Christopher M De Sa, Sen Wu, Daniel Selsam, and Christopher Ré. Data programming: Creating large training sets, quickly. In *Advances in Neural Information Processing Systems*, pages 3567–3575, 2016.
- [55] Christopher Ré, Feng Niu, Pallavi Gudipati, and Charles Srisuwananukorn. Overton: A data system for monitoring and improving machine-learned products. In *Proceedings of the 10th Annual Conference on Innovative Data Systems Research*, 2020.
- [56] Sebastian Riedel, Limin Yao, and Andrew McCallum. Modeling relations and their mentions without labeled text. In *Joint European Conference on Machine Learning and Knowledge Discovery in Databases*, pages 148–163. Springer, 2010.
- [57] Khaled Saab, Jared Dunnmon, Roger Goldman, Alex Ratner, Hersh Sagreiya, Christopher Ré, and Daniel Rubin. Doubly weak supervision of deep learning models for head ct. In *International Conference on Medical Image Computing and Computer-Assisted Intervention*, pages 811–819. Springer, 2019.
- [58] Tim Salimans, Ian Goodfellow, Wojciech Zaremba, Vicki Cheung, Alec Radford, and Xi Chen. Improved techniques for training gans. *Advances in neural information processing systems*, 29: 2234–2242, 2016.
- [59] Changho Shin, Wunfred Li, Harit Vishwakarma, Nicholas Roberts, and Frederic Sala. Universalizing weak supervision. *International Conference on Learning Representations (ICLR)*, 2022.
- [60] J. Stallkamp, M. Schlipsing, J. Salmen, and C. Igel. Man vs. computer: Benchmarking machine learning algorithms for traffic sign recognition. *Neural Networks*, (0):–, 2012. ISSN 0893-6080. doi: 10.1016/j.neunet.2012.02.016. URL <http://www.sciencedirect.com/science/article/pii/S0893608012000457>.
- [61] Kiran K Thekumparampil, Ashish Khetan, Zinan Lin, and Sewoong Oh. Robustness of conditional gans to noisy labels. In S. Bengio, H. Wallach, H. Larochelle, K. Grauman, N. Cesa-Bianchi, and R. Garnett, editors, *Advances in Neural Information Processing Systems*, volume 31. Curran Associates, Inc., 2018. URL <https://proceedings.neurips.cc/paper/2018/file/565e8a413d0562de9ee4378402d2b481-Paper.pdf>.

- [62] Paroma Varma and Christopher Ré. Snuba: automating weak supervision to label training data. *Proceedings of the VLDB Endowment*, 12(3):223–236, 2018.
- [63] Xiaosong Wang, Yifan Peng, Le Lu, Zhiyong Lu, Mohammadhadi Bagheri, and Ronald M Summers. Chestx-ray8: Hospital-scale chest x-ray database and benchmarks on weakly-supervised classification and localization of common thorax diseases. In *Proceedings of the IEEE conference on computer vision and pattern recognition*, pages 2097–2106, 2017.
- [64] Han Xiao, Kashif Rasul, and Roland Vollgraf. Fashion-mnist: a novel image dataset for benchmarking machine learning algorithms, 2017.
- [65] Xin Yi, Ekta Walia, and Paul Babyn. Generative adversarial network in medical imaging: A review. *Medical image analysis*, 58:101552, 2019.
- [66] Jieyu Zhang, Yue Yu, Yinghao Li, Yujing Wang, Yaming Yang, Mao Yang, and Alexander Ratner. Wrench: A comprehensive benchmark for weak supervision. In *Thirty-fifth Conference on Neural Information Processing Systems Datasets and Benchmarks Track (Round 2)*, 2021.
- [67] Jieyu Zhang, Cheng-Yu Hsieh, Yue Yu, Chao Zhang, and Alexander Ratner. A survey on programmatic weak supervision, 2022.

## Appendix

---

**Algorithm 1** Pseudocode for the proposed WSGAN loss term which is added to the basic InfoGAN loss. Input images and LFs are assumed to be filtered to only contain samples with at least 1 non-abstaining LF vote.

---

```
input: Batch of real images  $X$  and one-hot encoded LFs  $\Lambda$ , label model  $L$ , networks  $Q, A, F_1, F_2$ ,  
WSGAN mode  $m$ , number of classes  $C$ , current epoch  $i$ ,  $\gamma$  decay parameter.  
 $\hat{b}, Z = Q(X)$  # get predicted code and image features  $Z$   
if  $m == \text{"vector"}$ :  
     $\theta = A_\theta()$  # WSGAN-vector: get weight vector.  
else:  
     $\theta = A(Z.detach())$  # WSGAN-encoder: predict weights using image features  $Z$ .  
 $\hat{y} = L(\Lambda, \theta)$  # Get label estimate from labelmodel using weights  $\theta$ .  
# Compute cross-entropy losses  
 $loss = celloss(F_1(\hat{b}), \hat{y}.detach())$   
 $loss += celloss(F_2(\hat{y}), \hat{b}.detach())$   
 $loss += C/(i \times \gamma + 1)mse(\theta, \bar{1} \times 0.5)$  # add decaying loss keeping weights uniform.  
return  $loss$ 
```

---

## A Implementation Details and Complexity

**Models** *Generator G, Discriminator D, and auxilliary model Q:* Figures 5 and 4 show the simple DCGAN [51] based generator and discriminator architectures we use in WSGAN for experiments with  $32 \times 32$  images As mentioned in the main paper,  $Q$  and  $D$  are neural networks that generally share all convolutional layers, with a final fully connected layer to output predictions. We follow the same structure in our experiments. We set the dimension of the noise variable  $z$  to 100, and of  $b$  equal to the number of classes. We sample  $z$  from a normal distribution and  $b$  from a uniform discrete distribution.

*Accuracy Encoder A:* For WSGAN-Vector,  $A$  is simply a parameter vector of the same length as the number of labeling functions. For WSGAN-Encoder, we use image features obtained from the shared convolutional layers of  $Q$  and  $D$ , which we detach from the computational graph before passing them on to an MLP prediction head. For images with  $32 \times 32$  pixels, the feature vector obtained from the shared convolutional layers is of size  $512 * 16$ . The MLP head of  $A$  is set to have three hidden layers of size (256, 128, 64), with ReLU activations, and an output layer the size of the number of labeling functions followed by a sigmoid function.

*Mappings  $F_1, F_2$ :* We set  $F_1$  and  $F_2$  to each be simple linear models with a softmax at the output, and set the input and output size of each to the number of classes.

**(WS)GAN Training** We use the same hyperparameter settings for all datasets. We train all GANs for a maximum of 200 epochs. We use a batch size of 16 and find that a lower batch size leads to more frequent convergence of the generator and discriminator. We also conducted ablation experiments with a batch size of 8 and 32 and found no significant difference in FID image generation quality or label model accuracy. For WSGAN, we use four optimizers, one for each of the different loss terms: discriminator training, generator training, the Info loss term, and the WSGAN loss term. We use Adam for all optimizers and set the learning rates as follows:  $4 \times 10^{-4}$  for  $D$ ,  $1 \times 10^{-4}$  for  $G$ ,  $1 \times 10^{-4}$  for the info loss term, and  $8 \times 10^{-5}$  for the WSGAN loss term. We follow the same settings for InfoGAN training for the components shared with WSGAN.

Furthermore, we find that employing discriminator label flipping (randomly calling a tiny percentage of real samples fake and vice versa) and label smoothing (adding small amounts of noise to the real target of 1.0 and fake target of 0.0) stabilizes and improves GAN training. However, we were unable to completely avoid the occasional failure of the GAN component of WSGAN. Fortunately, monitoring the generator and discriminator losses, inspecting the quality of generated images, or tracking image quality metrics such as FID allows one to easily discard failed runs or to pick model checkpoints from earlier iterations before a failure, without requiring labeled data.

Layer (type:depth-idx)	Output Shape	Param #
InfoCDiscriminator	--	--
└Sequential: 1-1	[16, 512, 4, 4]	--
└Conv2d: 2-1	[16, 64, 32, 32]	1,792
└LeakyReLU: 2-2	[16, 64, 32, 32]	--
└Conv2d: 2-3	[16, 64, 16, 16]	65,600
└LeakyReLU: 2-4	[16, 64, 16, 16]	--
└Conv2d: 2-5	[16, 128, 16, 16]	73,856
└LeakyReLU: 2-6	[16, 128, 16, 16]	--
└Conv2d: 2-7	[16, 128, 8, 8]	262,272
└LeakyReLU: 2-8	[16, 128, 8, 8]	--
└Conv2d: 2-9	[16, 256, 8, 8]	295,168
└LeakyReLU: 2-10	[16, 256, 8, 8]	--
└Conv2d: 2-11	[16, 256, 4, 4]	1,048,832
└LeakyReLU: 2-12	[16, 256, 4, 4]	--
└Conv2d: 2-13	[16, 512, 4, 4]	1,180,160
└LeakyReLU: 2-14	[16, 512, 4, 4]	--
└Dropout: 2-15	[16, 512, 4, 4]	--
└Sequential: 1-2	[16, 1, 1, 1]	--
└Conv2d: 2-16	[16, 1, 1, 1]	8,192

Figure 4: The DCGAN discriminator architecture used in our experiments with 32 x 32 images.

**End Model Training** For all datasets, we train a ResNet-18 [27] for 100 epochs, using Adam and a learning rate scheduler. The learning rate scheduler uses a small validation set to make adjustments to the learning rate.

**Image Augmentation** We use the following random image augmentation functions during GAN and endmodel training for color images: random crop and resize (cropping out a maximum height/width of 13%), random sharpness adjustment ( $p = 0.2$ ), random color jitter, and random Gaussian blur ( $p = 0.1$ ).

**Complexity** WSGAN shares the same operations as InfoGAN and adds some additional steps on real samples that have at least one LF vote, which slightly increases the required computation. Recall that  $C$  denotes the number of classes,  $m$  the number of LFs, and  $x$  an image of a real sample. Further, let  $n_w$  denote the number of samples that have at least one weak label vote from any LF, let  $q$  denote the number of steps required for a forward pass through  $Q$  to obtain image features and the discrete code prediction, and  $a$  denote the number of steps for a forward pass through the MLP  $A$ . For a forward pass, WSGAN increases the complexity compared to InfoGAN in each epoch by  $\Theta(n_w(a + q + m + 2C^2 + C(m + 8)))$ . Note that  $q$  may be eliminated for the forward pass through careful implementation as the image features are already obtained for the basic InfoGAN update. In practice, in our experiments the computational overhead, including for additional data loading of the LFs, leads to a modest increase in runtime (measured in bps, denoting batches per second) of the weakly supervised WSGAN over the unsupervised InfoGAN, as follows. InfoGAN: 14bps, WSGAN Encoder: 7.8bps, WSGAN Vector: 8.6bps (NVIDIA RTX A6000, batch size 16). In terms of parameters, WSGAN shares the same generator  $G$  and discriminator components  $D, Q$  as InfoGAN, and adds additional label model parameters. The overall number of parameters in our experiments with 32 x 32 images are: InfoGAN 6.7M, WSGAN 8.8M.

## B Dataset Details

- *CIFAR10* contains 32x32 color images of 10 different classes. We create two different CIFAR10 subsets. One set (used for experiments CIFAR10-C,D) uses the full training set of CIFAR10 (minus 300 samples held out for downstream validation), while the second (used for experiments CIFAR10-A,B,E,F) is a random subset of 30,000 training images.
- *MNIST* and *FashionMNIST* both contain 28x28 grayscale images, which we resize to 32x32. For both, we use a random sample of 30,000 images from the training data for our

Layer (type:depth-idx)	Output Shape	Param #
DCGeneratorThree	--	--
├Linear: 1-1	--	2
├Sequential: 1-2	[16, 3, 32, 32]	--
│├ConvTranspose2d: 2-1	[16, 512, 4, 4]	901,632
│├BatchNorm2d: 2-2	[16, 512, 4, 4]	1,024
│├ReLU: 2-3	[16, 512, 4, 4]	--
│├ConvTranspose2d: 2-4	[16, 256, 8, 8]	2,097,408
│├BatchNorm2d: 2-5	[16, 256, 8, 8]	512
│├ReLU: 2-6	[16, 256, 8, 8]	--
│├ConvTranspose2d: 2-7	[16, 128, 16, 16]	524,416
│├BatchNorm2d: 2-8	[16, 128, 16, 16]	256
│├ReLU: 2-9	[16, 128, 16, 16]	--
│├ConvTranspose2d: 2-10	[16, 64, 32, 32]	131,136
│├BatchNorm2d: 2-11	[16, 64, 32, 32]	128
│├ReLU: 2-12	[16, 64, 32, 32]	--
│├ConvTranspose2d: 2-13	[16, 3, 32, 32]	1,731
│├Tanh: 2-14	[16, 3, 32, 32]	--

Figure 5: The DCGAN generator architecture used in our experiments with 32x32 images.



Figure 6: Synthetic images and pseudolabels generated by the proposed WSGAN, learned from weakly supervised CIFAR10. We note that WSGAN is able to generate images and estimate their labels, even for images where no weak supervision sources provide information (see end of Section 3.1 for details).

experiments. SSL-based labeling functions are fine-tuned on small, random subsets of the remaining training data of each dataset.

- *GTSRB* contains 64x64 color images of German traffic signs. We use 22,640 random images from the full training dataset during our experiments, while random subsets of the remaining images in the original training data are used to finetune the SSL-based labeling functions.
- The original *DomainNet* [50] dataset contains 345 classes of images in 6 different domains<sup>5</sup>. As our dataset, following Mazzetto et al. [43] we use the images in the real domain and select the 10 classes with the largest number of instances in this domain. Because of the small size of the resulting dataset, we resize the images to 32 x 32 in our experiments.
- *Animals with Attributes 2* (AwA2) [43] is an image dataset with known general attributes for each class, divided into 40 seen and 10 unseen classes. Because of the small size of the resulting dataset once LFs are created, we resize the images to 32 x 32 in our experiments.

## B.1 Labeling Function Details

- *Synthetic*: based on the true class label, we create synthetic, unipolar LFs via the following procedure: for each LF, we sample a class label, an error rate, and a propensity (i.e., the percentage of samples where the LF casts a vote, also referred to as coverage). Given the target label, we then sample true positives and false positives at random to achieve the desired LF accuracy and propensity.

<sup>5</sup>Real, painting, sketch, clipart, infographic, quickdraw.

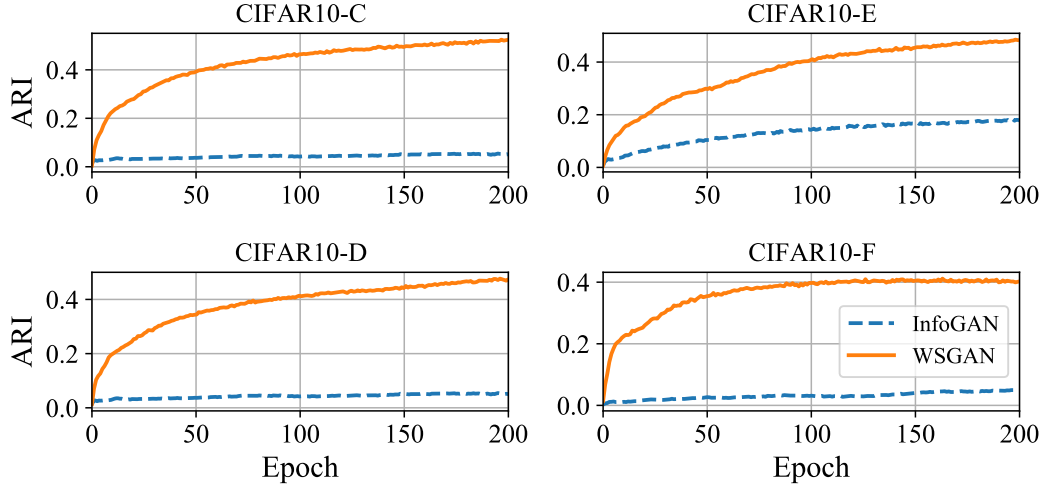


Figure 7: We here show the Adjusted Rand Index (ARI) for the additional CIFAR experiments. The plots show the ARI between the unobserved class label  $y$  and the discrete code prediction by the auxiliary model  $Q(x)$  on real image  $x$ , during training. Weak supervision allows WSGAN to better uncover the latent class structure compared to an unsupervised InfoGAN.

- *Domain transfer*: these LFs are used in our DomainNet dataset experiments. We follow Mazzetto et al. [43], and derive weak supervision sources for a multiclass classification task of the real images contained in the DomainNet [50] dataset. First, we set our target domain to real images and select the 10 classes with the largest number of instances in this domain. As LFs, we then train classifiers using the selected classes within the remaining five domains, and apply these trained classifiers to the unseen images in the target domain of real images to obtain weak labels.
- *Attribute heuristics*: we create two sets of LFs for the Animals with Attributes 2 (AwA2) [43] image classification dataset. Following Mazzetto et al. [44, 43], we train one-vs-rest attribute classifiers using the 40 seen classes of the AwA2 dataset. These classifiers are applied to the 10 unseen classes to produce weak attribute labels. At this stage, we discard attribute classifiers which perform worse than random. We create an 85%/5%/10% train/validation/test split of the 10 unseen classes which we use to define decision trees to produce weak labels on the bases of weak attribute predictions. We create the 29 unipolar LFs for *AwA2-A* by training 3 one-vs-rest decision trees per each of the 10 classes on 100 random samples from the training set. To create a slightly easier set, we create the 32 unipolar LFs used in *AwA2-B* by training 80 decision trees, retaining one random tree specializing in each class, and then selecting all remaining ones where validation accuracy is higher than 0.65.
- *SSL-based*: The base representations are learned on unsupervised ImageNET with SimCLR [12]. The trained network is used to obtain features for our image datasets. We then train shallow MLP networks on a few hundred held-out samples to predict a randomly sampled target label at a randomly sampled target accuracy. The accuracy is validated to be within range of the target accuracy on another small amount of held-out data. Thus, during creation these unipolar LFs are never trained or evaluated on the WSGAN training data or the downstream test data.

## C Additional Experiments

We created additional weakly supervised image datasets based on CIFAR10 by varying the number of samples and the type of labeling function, see dataset details in Table 5. The proposed WSGAN approach outperforms related approaches in these experiments as well. The label model accuracy results are shown in Table 6, while additional metrics including F1 are shown in Section E. Image generation quality results are provided in Table 7. Finally, a comparison between the latent discrete variable of WSGAN and InfoGAN is given in Figure 7, which shows how the Adjusted Rand Index

Table 5: Additional datasets and labeling function (LF) characteristics used to evaluate the proposed WSGAN model. Acc denotes accuracy, while Coverage denotes the number of samples where the LF does not abstain.

Dataset	#Classes	#LFs	#Samples	Mean LF Acc	Min LF Acc	Max LF Acc	Mean Coverage	LF Type
CIFAR10-C	10	20	49700	0.747	0.621	0.879	0.048	Synthetic
CIFAR10-D	10	40	49700	0.760	0.621	0.898	0.052	Synthetic
CIFAR10-E	10	40	30000	0.761	0.624	0.896	0.056	Synthetic
CIFAR10-F	10	40	30000	0.728	0.531	0.912	0.046	SSL, finetuning

Table 6: Additional datasets: average posterior accuracy of various label models on training samples with at least one LF vote. We highlight the best result in **blue** and the second best result in **bold**.

Dataset	MV	DawidSkene	MeTaL	FS	Snorkel	WSGAN-Vector	WSGAN-Encoder
CIFAR10-C	0.762	<b>0.778</b>	0.751	0.764	0.757	<b>0.778</b>	<b>0.796</b>
CIFAR10-D	0.831	<b>0.861</b>	0.819	0.805	0.812	0.854	<b>0.865</b>
CIFAR10-E	0.865	<b>0.902</b>	0.845	0.827	0.849	0.898	<b>0.917</b>
CIFAR10-F	0.687	0.601	0.682	0.677	0.678	<b>0.691</b>	<b>0.702</b>

evolves between the unobserved class labels and the latent discrete variable modeled by auxiliary model  $Q$ .

## D Additional Baselines

We compare against two additional baselines. First, we train a generative model that is conditioned on pseudolabel information with the aim of improving image generation performance; we use pseudolabels provided by established weak-supervision label models in this role. Second, we use a basic generative model to produce synthetic samples that augment a downstream classifier (with weak labels provided by outputs of weak supervision sources applied to the synthetic images). These two baselines represent the straightforward way to use weak supervision to improve generative modeling (and vice-versa). We observe that such naive combinations struggle compared to our proposed approach, further motivating the importance of the interface in WSGAN.

### D.1 Image Generation with Pseudolabels

As an additional GAN baseline to our proposed WSGAN, we slightly adapt an Auxiliary Classifier Generative Adversarial Network (ACGAN) [48] to condition it on pseudolabels. The ACGAN is run on all data, but the auxiliary loss on real data with pseudolabels is only used for samples where at least one labeling function does not abstain. We create two versions: (1) using probabilistic pseudolabels with a soft cross-entropy loss, and (2) another using *hard/crisp* labels with a cross-entropy loss. To provide the strongest possible baseline in this experiment, we obtain the pseudolabels via the Dawid-Skene label model as it attains the best performance on average over all datasets compared to other related label models. Results are provided in Table 8, showing that this baseline approach is frequently unable to overcome the noise in the pseudolabels to improve over the InfoGAN results, and that it does not perform better than WSGAN with an encoder. Furthermore, it was much more difficult to successfully fit this approach to data and many runs had to be discarded as the quality of the generator collapsed early during training.

Table 7: Additional datasets: color image generation quality measured by average Fréchet Inception Distance (FID). The best scores for each dataset are highlighted in **blue**.

Dataset	InfoGAN	WSGAN-V	WSGAN-E
CIFAR10-C	33.64	<b>24.11</b>	26.00
CIFAR10-D	33.64	24.09	<b>23.78</b>
CIFAR10-E	28.93	<b>21.97</b>	22.63
CIFAR10-F	33.50	24.59	<b>22.54</b>

Table 8: A comparison to using an ACGAN with pseudolabels. Image generation quality is measured by average Fréchet Inception Distance (FID). The best scores for each dataset are highlighted in **blue**.

Dataset	InfoGAN	ACGAN	ACGAN (crisp)	WSGAN-V	WSGAN-E
AwA2 - A	41.62	51.32	47.21	36.74	<b>34.71</b>
AwA2 - B	41.62	53.73	50.03	36.79	<b>34.52</b>
DomainNet	51.88	61.96	47.32	51.16	<b>45.6</b>
CIFAR10-A	28.93	79.15	25.53	25.7	<b>22.71</b>
CIFAR10-C	33.64	36.53	26.61	<b>24.11</b>	26.0
CIFAR10-D	33.64	36.81	45.1	24.09	<b>23.78</b>
CIFAR10-E	28.93	80.43	33.05	<b>21.97</b>	22.63

Table 9: Baseline comparisons using an InfoGAN to create synthetic images, applying LFs to the synthetic images, and then using established label models to synthesize the weak labels in to a pseudolabel resulting in weakly labeled fake images. The table shows the change in test accuracy by augmenting the downstream classifier training data with such 1,000 synthetic images and corresponding pseudo labels. Experiments are conducted on a subset of the datasets where labeling functions can be applied to synthetic images.

Dataset	WSGAN	InfoGAN + Snorkel	InfoGAN + DawidSkene
AwA2 - A	0.79%	-0.63%	-1.26%
AwA2 - B	3.90%	-1.01%	-1.77%
DomainNet	1.50%	0.02%	-3.14%

## D.2 Data Augmentation for Downstream Classification with Synthetic Images

In this experiment, we augment the training set for a downstream classifier with synthetic images. As baselines, we generate synthetic images  $\tilde{x}$  with an InfoGAN, and then apply the image labeling functions  $\lambda$  to the generated images to obtain LF votes  $\lambda(\tilde{x})$ . Pseudolabels for the synthetic images are then obtained by fitting label models to the real training data and then applying the label models to the labeling function outputs on the synthetic data. Table 9 compares InfoGAN + Snorkel and InfoGAN + DawidSkene baselines to the improvements in test accuracy obtained by using WSGAN and shows that we were unable to obtain improvements in downstream accuracy with the baselines, possibly due to performance of the InfoGAN on these small datasets.

Table 10: In this table, we include standard deviations for the posterior accuracy of various label models on training samples with at least one LF vote, computed over five random runs. Due to a limited computational budget, we were unable to accumulate five runs for all datasets and model combinations.

Dataset	DawidSkene	MeTaL	FS	Snorkel	WSGAN-Encoder
AwA2 - A	0.607( $\pm 0.029$ )	0.632( $\pm 0.002$ )	0.615( $\pm 0.003$ )	0.641( $\pm 0.001$ )	<b>0.681</b> ( $\pm 0.011$ )
DomainNet	<b>0.658</b> ( $\pm 0.000$ )	0.487( $\pm 0.004$ )	0.635( $\pm 0.000$ )	0.499( $\pm 0.015$ )	0.643( $\pm 0.003$ )
MNIST	0.729( $\pm 0.000$ )	0.766( $\pm 0.001$ )	0.773( $\pm 0.000$ )	0.766( $\pm 0.001$ )	<b>0.813</b> ( $\pm 0.004$ )
FashionMNIST	0.717( $\pm 0.002$ )	0.730( $\pm 0.001$ )	0.734( $\pm 0.001$ )	0.729( $\pm 0.001$ )	<b>0.744</b> ( $\pm 0.002$ )
GTSRB	0.619( $\pm 0.001$ )	<b>0.815</b> ( $\pm 0.002$ )	0.679( $\pm 0.001$ )	<b>0.814</b> ( $\pm 0.000$ )	<b>0.823</b> ( $\pm 0.001$ )
CIFAR10-A	<b>0.850</b> ( $\pm 0.001$ )	0.806( $\pm 0.001$ )	0.800( $\pm 0.000$ )	0.807( $\pm 0.002$ )	<b>0.874</b> ( $\pm 0.002$ )
CIFAR10-B	0.677( $\pm 0.000$ )	0.708( $\pm 0.001$ )	0.708( $\pm 0.000$ )	0.707( $\pm 0.000$ )	<b>0.731</b> ( $\pm 0.004$ )

Table 11: Weighted mean average precision of various label models on training samples with at least one LF vote. We highlight the best result in **blue** and the second best result in **bold**.

Dataset	MV	DawidSkene	MeTaL	FS	Snorkel	WSGAN-Vector	WSGAN-Encoder
AwA2 - A	0.616	0.661	0.653	0.627	0.653	<b>0.672</b>	<b>0.737</b>
AwA2 - B	0.591	0.652	0.662	0.642	0.668	<b>0.681</b>	<b>0.743</b>
DomainNet	0.599	<b>0.702</b>	0.630	0.654	0.621	0.679	<b>0.795</b>
MNIST	0.684	0.772	0.784	0.765	0.785	<b>0.792</b>	<b>0.870</b>
FashionMNIST	0.620	0.712	0.691	0.686	0.692	<b>0.703</b>	<b>0.742</b>
GTSRB	0.718	0.731	0.761	0.714	<b>0.772</b>	0.768	<b>0.808</b>
CIFAR10-A	0.796	0.866	0.855	0.838	0.854	<b>0.878</b>	<b>0.912</b>
CIFAR10-B	0.594	0.659	0.658	0.631	0.666	<b>0.678</b>	<b>0.732</b>
CIFAR10-C	0.664	0.763	0.758	0.737	0.751	<b>0.780</b>	<b>0.825</b>
CIFAR10-D	0.788	0.896	0.889	0.876	0.878	<b>0.901</b>	<b>0.908</b>
CIFAR10-E	0.880	<b>0.954</b>	0.942	0.924	0.940	0.950	<b>0.959</b>
CIFAR10-F	0.561	0.658	0.66	0.647	0.659	<b>0.675</b>	<b>0.708</b>

## E Additional Metrics

We provide additional metrics for the label model comparisons shown in Table 2 in the main paper. Again, results are averaged over 4 random runs. Table 12 shows the weighted F1 score, an average over all classes weighted by the support of each class. Table 11 shows weighted mean average precision, a metric that summarizes the precision-recall curve across all classes. We compute the average precision individually for each class (one vs. rest) and then aggregate the scores by summing them weighted by the support of each class to produce the weighted mean average precision score.

Table 12: Weighted F1 score of various label models on training samples with at least one LF vote. The F1 is computed separately for each class and then averaged weighted by the support of each class. We highlight the best result in **blue** and the second best result in **bold**.

Dataset	MV	DawidSkene	MeTaL	FS	Snorkel	WSGAN-Vector	WSGAN-Encoder
AwA2 - A	0.641	<b>0.665</b>	0.62	0.619	0.636	0.637	<b>0.684</b>
AwA2 - B	0.604	<b>0.661</b>	0.58	0.597	0.593	<b>0.664</b>	<b>0.672</b>
DomainNet	0.603	<b>0.655</b>	0.443	0.622	0.468	<b>0.654</b>	<b>0.634</b>
MNIST	0.756	0.716	0.746	0.755	0.746	<b>0.764</b>	<b>0.795</b>
FashionMNIST	0.706	0.691	0.698	0.705	0.698	<b>0.710</b>	<b>0.715</b>
GTSRB	<b>0.802</b>	0.616	0.800	0.628	0.799	<b>0.801</b>	<b>0.811</b>
CIFAR10-A	0.824	<b>0.850</b>	0.797	0.796	0.798	<b>0.851</b>	<b>0.872</b>
CIFAR10-B	0.712	0.672	0.702	0.703	0.702	<b>0.720</b>	<b>0.727</b>
CIFAR10-C	0.726	<b>0.741</b>	0.723	0.713	0.718	<b>0.738</b>	<b>0.759</b>
CIFAR10-D	0.809	<b>0.839</b>	0.791	0.784	0.781	0.834	<b>0.844</b>
CIFAR10-E	0.864	<b>0.901</b>	0.843	0.825	0.839	<b>0.899</b>	<b>0.916</b>
CIFAR10-F	0.684	0.609	0.677	0.675	0.674	<b>0.688</b>	<b>0.699</b>

## F Theoretical Justification

We provide additional setup and proofs for our two theoretical claims.

### F.1 Claim (1)

Our goal is to derive a generalization bound; that is, an upper bound on  $|\hat{\mathbb{R}}_{\mathcal{D}} - \mathbb{R}_{\mathcal{D}}|$ . In words, this is the gap between the loss on a sample drawn from the true distribution and the empirical loss we obtained by training on the weakly-supervised dataset with unlabeled data sampled from the generative model.

**Mixture of Gaussians** Recall that  $D$  is the joint distribution of the unlabeled and labeled points. Let's call the unlabeled data marginal distribution  $D_X$ . Then, we make the assumption that  $D_X$  is a mixture of  $k$  Gaussians. Here, there is some relationship between the mixtures and the two classes, but we need not further specify it. Using the result [2], we get that the number of samples needed to learn  $D_X$  up to  $\varepsilon$  in total variation distance is  $\tilde{\Theta}(kd^2/\varepsilon^2)$ .

Note that in fact this expression hides some polylogarithmic terms. However, for simplicity, we're going to ignore these terms and just pretend that the necessary bound is  $c_G kd^2/\varepsilon^2$ , where  $c_G$  is some constant for learning a density.

Based on this, we'll make the following assumption. We perform density estimation on  $n_1$  samples from  $D_X$  and obtain some model  $g$  such that distribution of  $g$  (we'll abuse notation and just refer to this as the model itself  $g$ ) and  $D_X$  satisfies

$$d_{\text{TV}}(D_X, g) \leq d \sqrt{\frac{c_G k}{n_1}}. \quad (5)$$

So now we have control over one marginal (the unlabeled data). Let's work on the conditional term next.

**Majority Vote** For simplicity, let's assume that we use majority vote as the aggregation scheme for the  $m$  labeling functions. We make the following assumptions. The labeling functions have accuracy  $1/2 + \alpha$ , for some  $\alpha \in (0, 1/2]$ , in the following sense. For any datapoint  $(X, Y)$ , the probability of a labeling function guessing the value of  $Y$  correctly is  $1/2 + \alpha$ , and the probability of any guessing wrong is  $1/2 - \alpha$ . This holds for all values of  $X$ . Note: these are very strong assumptions.

The probability that we make a mistake, e.g., that majority vote aggregates votes to 0 when  $Y = 1$  or vice-versa is given by the binomial CDF  $F(m/2, m, \alpha + 1/2)$ , which has the following simple bound that follows from Hoeffding's inequality,

$$F(m/2, m, \alpha + 1/2) \leq \exp\left(-2m\left(\alpha + 1/2 - \frac{m/2}{m}\right)^2\right) = \exp(-2m\alpha^2).$$

With the above, as  $D_{Y|X}$  is a Bernoulli random variable, we can directly upper bound the total variation distance between  $D_{Y|X}$  and  $D_{\hat{Y}|X}$ :

$$d_{\text{TV}}(D_{Y|X}, D_{\hat{Y}|X}) \leq \exp(-2m\alpha^2). \quad (6)$$

**Joint Distribution** Now we have some control over the generative model's error (from the density estimation bound) and some control over the label recovery (from the above bound resulting from majority vote). Now we put it together. First, we write down some useful inequalities between the total variation distance and the Hellinger distance [20] (Prop 2.10). These are, for densities  $p, q$ ,

$$D_{\text{hel}}(p, q) \leq \sqrt{2d_{\text{TV}}(p, q)} \quad (7)$$

and

$$d_{\text{TV}}(p, q) \leq D_{\text{hel}}(p, q) \sqrt{1 - D_{\text{hel}}(p, q)^2/4}. \quad (8)$$

We use  $p$  as the density for  $\mathcal{D}$  and  $q$  as the density for  $\hat{\mathcal{D}}$ , and write  $p = p_1(x)p_2(y|x)$ ,  $q = q_1(x)q_2(y|x)$ . First, using Eq. (5) and Eq. (7), we have that

$$D_{\text{hel}}(\mathcal{D}_X, g) \leq \sqrt{2d_{\text{TV}}(\mathcal{D}_X, g)} \leq \left( \frac{4c_G k d^2}{n_1} \right)^{\frac{1}{4}}. \quad (9)$$

Then, using Eq. (6) and Eq. (7), we get

$$D_{\text{hel}}(D_{Y|X}, D_{\hat{Y}|X}) \leq \sqrt{2d_{\text{TV}}(D_{Y|X}, D_{\hat{Y}|X})} \leq \sqrt{2 \exp(-2m\alpha^2)} = \sqrt{2} \exp(-m\alpha^2). \quad (10)$$

Next,

$$\begin{aligned} D_{\text{hel}}(\mathcal{D}, \hat{\mathcal{D}}) &= \int \int (\sqrt{p_1(x)p_2(y|x)} - \sqrt{q_1(x)q_2(y|x)})^2 dy dx \\ &= \int \int \left( p_1(x)p_2(y|x) + q_1(x)q_2(y|x) - 2\sqrt{p_1(x)p_2(y|x)q_1(x)q_2(y|x)} \right) dy dx \\ &= 2 - 2 \int \int \sqrt{p_1(x)p_2(y|x)q_1(x)q_2(y|x)} dy dx \\ &= 2 - 2 \int \sqrt{p_1(x)q_1(x)} \left( 1 - \frac{1}{2} D_{\text{hel}}(p_2, q_2) \right) dx \\ &\leq 2 - 2 \int \sqrt{p_1(x)q_1(x)} \left( 1 - \frac{\sqrt{2}}{2} \exp(-m\alpha^2) \right). \end{aligned}$$

Note that here, we use the fact that our bound holds for all conditional distributions regardless of  $x$ . Continuing,

$$\begin{aligned} D_{\text{hel}}(\mathcal{D}, \hat{\mathcal{D}}) &\leq 2 - 2 \int \sqrt{p_1(x)q_1(x)} \left( 1 - \frac{\sqrt{2}}{2} \exp(-m\alpha^2) \right) \\ &= 2 - 2 \left( 1 - \frac{1}{2} D_{\text{hel}}(p_1, q_1) \right) \left( 1 - \frac{\sqrt{2}}{2} \exp(-m\alpha^2) \right) \\ &\leq 2 - 2 \left( 1 - \frac{1}{2} \left( \frac{4c_G k d^2}{n_1} \right)^{\frac{1}{4}} \right) \left( 1 - \frac{\sqrt{2}}{2} \exp(-m\alpha^2) \right) \\ &= \left( \frac{4c_G k d^2}{n_1} \right)^{\frac{1}{4}} + \sqrt{2} \exp(-m\alpha^2) - \left( \frac{c_G k d^2}{n_1} \right)^{\frac{1}{4}} \exp(-m\alpha^2). \end{aligned}$$

Now we apply Eq. (8) to get the bound back into the total variation distance setting. We have

$$\begin{aligned} d_{\text{TV}}(\mathcal{D}, \hat{\mathcal{D}}) &\leq D_{\text{hel}}(\mathcal{D}, \hat{\mathcal{D}}) \sqrt{1 - D_{\text{hel}}(\mathcal{D}, \hat{\mathcal{D}})^2/4} \leq D_{\text{hel}}(\mathcal{D}, \hat{\mathcal{D}}) \\ &\leq \left( \frac{4c_G k d^2}{n_1} \right)^{\frac{1}{4}} + \sqrt{2} \exp(-m\alpha^2) - \left( \frac{c_G k d^2}{n_1} \right)^{\frac{1}{4}} \exp(-m\alpha^2) \\ &\leq \left( \frac{4c_G k d^2}{n_1} \right)^{\frac{1}{4}} + \sqrt{2} \exp(-m\alpha^2). \end{aligned} \quad (11)$$

**Bounding the Risk** The final task is to bound the risk. First, suppose we are training a classifier chosen from a function class  $\mathcal{F}$ , trained on  $n_2$  independently-drawn data points. Then, a standard result is that with probability at least  $1 - \delta$ ,

$$\sup_{f \in \mathcal{F}} |\hat{\mathbb{R}}_{\mathcal{D}}(f) - \mathbb{R}_{\mathcal{D}}(f)| \leq 2\mathfrak{R} + \sqrt{\frac{\log(1/\delta)}{2n_2}}. \quad (12)$$

Here,  $\mathfrak{R}$  is the Rademacher complexity of the function class. However, the above is for training on samples from the true distribution. Instead, we can write

$$\begin{aligned} |\hat{\mathbb{R}}_{\hat{\mathcal{D}}} - \mathbb{R}_{\mathcal{D}}| &= |\hat{\mathbb{R}}_{\hat{\mathcal{D}}} - \mathbb{R}_{\hat{\mathcal{D}}} + \mathbb{R}_{\hat{\mathcal{D}}} - \mathbb{R}_{\mathcal{D}}| \\ &\leq |\hat{\mathbb{R}}_{\hat{\mathcal{D}}} - \mathbb{R}_{\hat{\mathcal{D}}}| + |\mathbb{R}_{\hat{\mathcal{D}}} - \mathbb{R}_{\mathcal{D}}|. \end{aligned}$$

For the right-hand term, we have the following:

$$\begin{aligned} |\mathbb{R}_{\hat{\mathcal{D}}} - \mathbb{R}_{\mathcal{D}}| &= \left| \int \ell(f(x), y) |p(x, y) - q(x, y)| d\mu \right. \\ &\leq B_\ell d_{\text{TV}}(\hat{\mathcal{D}}, \mathcal{D}). \end{aligned}$$

Then, putting this together with the expression in Eq. (11) into Eq. (12), we get that, with probability at least  $1 - \delta$ ,

$$\begin{aligned} \sup_{f \in \mathcal{F}} |\hat{\mathbb{R}}_{\hat{\mathcal{D}}}(f) - \mathbb{R}_{\mathcal{D}}(f)| &\leq (\sup_{f \in \mathcal{F}} |\hat{\mathbb{R}}_{\hat{\mathcal{D}}} - \mathbb{R}_{\hat{\mathcal{D}}}| + |\mathbb{R}_{\hat{\mathcal{D}}} - \mathbb{R}_{\mathcal{D}}|) \\ &\leq 2\mathfrak{R} + \sqrt{\frac{\log(1/\delta)}{2n_2}} + B_\ell d_{\text{TV}}(\hat{\mathcal{D}}, \mathcal{D}) \\ &\leq 2\mathfrak{R} + \sqrt{\frac{\log(1/\delta)}{2n_2}} + B_\ell \left( \frac{4c_G k d^2}{n_1} \right)^{\frac{1}{4}} + B_\ell \sqrt{2} \exp(-m\alpha^2). \end{aligned} \quad (13)$$

**Interpreting the Bound** In Eq. (13), we saw that

$$\sup_{f \in \mathcal{F}} |\hat{\mathbb{R}}_{\hat{\mathcal{D}}}(f) - \mathbb{R}_{\mathcal{D}}(f)| \leq 2\mathfrak{R} + \sqrt{\frac{\log(1/\delta)}{2n_2}} + B_\ell \left( \frac{4c_G k d^2}{n_1} \right)^{\frac{1}{4}} + B_\ell \sqrt{2} \exp(-m\alpha^2).$$

Now let's interpret this result piece-by-piece. The terms are the following

- The Rademacher complexity of the function class, which is present in the standard generalization bound.
- An estimation error term as a function of how much data we have to train our classifier  $n_2$ . It has the standard rate  $1/\sqrt{n_2}$ . Again, this is standard in any bound.
- A penalty term due to the generative model usage. It tells us how much we lose by training on generated data rather than (unlabeled) data from the true distribution. It scales as  $n_1^{-1/4}$ , where  $n_1$  is the number of samples of unlabeled data used to train the generative model. Note also the dependence on the number of mixture components and dimension.
- A penalty term due to weak supervision. It tells us what we lose by using estimated (pseudo)labels rather than true labels; we note that the penalty scales exponentially in the number of labeling functions  $m$ , but is slowed down by small  $\alpha$ , as our accuracies are  $\alpha$  better than random.

## F.2 Claim (2)

Our proof of claim (2) uses the setting of Thekumparampil et al. [61], which introduces RCGAN. RCGAN is a conditional GAN architecture that corrupts the label before passing them to the discriminator by passing the true labels through a noisy channel. The authors provide a multiplicative approximation bound between the GAN loss under the unobserved true labels and the loss under the noisy labels. This noisy channel model acts as a nice model of the label generating process of weak supervision. Using this noisy channel model, we can control the amount of label corruption to match that of weak supervision.

Following the setup of Thekumparampil et al. [61], we define a function that multiplies a one-hot encoded true label vector by a right-stochastic matrix  $C \in \mathbb{R}^{2 \times 2}$  where  $C_{i,j} = P(\tilde{y}_j | y_i)$ —this is our noisy channel. This induces a joint distribution  $\tilde{P}_{X, \tilde{Y}}$  for the examples  $x$  and noisy labels  $\tilde{y}$  from the conditional distribution defined by  $C$ . We restate the theorems of interest from Thekumparampil et al. [61] here, and proceed to adapt them to our problem setting.

**Theorem 1.** (Multiplicative bound on the total variation distance from Thekumparampil et al. [61].) *Let  $P_{X, Y}$  and  $Q_{X, Y}$  be two distributions over  $\mathcal{X} \times \{0, 1\}$  and let  $\tilde{P}_{X, \tilde{Y}}$  and  $\tilde{Q}_{X, \tilde{Y}}$  be the corresponding distributions with noisy labels from  $C$ . If  $C$  is full-rank, then*

$$d_{\text{TV}}(\tilde{P}, \tilde{Q}) \leq d_{\text{TV}}(P, Q) \leq \|C^{-1}\|_\infty d_{\text{TV}}(\tilde{P}, \tilde{Q}). \quad (14)$$

Theorem 1 says that the total variation distance between the true noisy distribution and the noisy generated distribution from RCGAN approximate its noiseless counterpart up to a factor of  $\|C^{-1}\|_\infty$ . Our goal is to construct  $C_{\epsilon_{MV}}$  to model the noise from weak supervision (in particular, majority vote) and show that it leads to a tighter bound than when we directly plug in the labels from a single LF into Theorem 1. To begin, consider the following parameterization of  $C$ , with  $\epsilon \in (0, 1/2)$ :

$$C_\epsilon = I_2 + \begin{bmatrix} -\epsilon & \epsilon \\ \epsilon & -\epsilon \end{bmatrix} = \begin{bmatrix} 1-\epsilon & \epsilon \\ \epsilon & 1-\epsilon \end{bmatrix}. \quad (15)$$

Here,  $\epsilon$  denotes the labeling error for each class. Given this parameterization, we obtain the following expression for  $\|C_\epsilon^{-1}\|_\infty$ .

$$\|C_\epsilon^{-1}\|_\infty = \left\| \begin{bmatrix} 1-\epsilon & \epsilon \\ \epsilon & 1-\epsilon \end{bmatrix}^{-1} \right\|_\infty \quad (16)$$

$$= |((1-\epsilon)^2 - \epsilon^2)^{-1}| \left\| \begin{bmatrix} 1-\epsilon & -\epsilon \\ -\epsilon & 1-\epsilon \end{bmatrix} \right\|_\infty \quad (17)$$

$$= (1-2\epsilon)^{-1} \quad (18)$$

Note that  $C_\epsilon$  is full-rank as it has a finite inverse. It is also clear that  $\|C_\epsilon^{-1}\|_\infty$  is a monotonically increasing function of  $\epsilon$ . That is to say that if we do something to decrease the labeling error  $\epsilon$ , then  $\|C_\epsilon^{-1}\|_\infty$  also decreases and we obtain a tighter bound. We will go on to derive an expression for the labeling error under majority vote with  $m$  LFs,  $\epsilon_{MV}$ , and show that it is smaller than the labeling error from a single LF,  $\epsilon_\lambda$ . Namely, we want find a condition where  $\epsilon_{MV} \leq \epsilon_\lambda$  holds and that majority vote leads to an improved Theorem 1 bound.

**Proposition 1.** (Total variation version.) *Let  $\epsilon_{MV}$  be the labeling error from majority vote from  $m$  LFs, where  $m \geq \frac{\log(1/\epsilon_\lambda)}{2(\frac{1}{2}-\epsilon_\lambda)^2}$ , whose individual labeling errors are each  $\epsilon_\lambda$ . Then the following holds*

$$d_{TV}(\tilde{P}_{MV}, \tilde{Q}_{MV}) \leq d_{TV}(P, Q) \leq \|C_{\epsilon_{MV}}^{-1}\|_\infty d_{TV}(\tilde{P}_{MV}, \tilde{Q}_{MV}) \leq \|C_{\epsilon_\lambda}^{-1}\|_\infty d_{TV}(\tilde{P}_{MV}, \tilde{Q}_{MV}).$$

*Proof.* We begin by deriving an upper bound on  $\epsilon_{MV}$ . We have LFs  $\{\lambda_i\}_{i=1}^m$  that each produce incorrect predictions with probability  $\epsilon_\lambda = \frac{1}{2} - \alpha$ , using  $\alpha$  as defined in Claim (1). Now, we need to show that the probability of producing incorrect predictions using majority vote with more label functions,  $\{\lambda_i\}_{i=1}^m$ , has error  $\epsilon_{MV} \leq \epsilon_\lambda$ . Define the event that  $\lambda_i$  is incorrect as follows:  $z_i = \mathbb{I}[\lambda_i \neq y]$ , then  $\mathbb{E}[\sum z_i] = m\epsilon_\lambda$ . Using this, we apply Hoeffding's bound to  $\epsilon_{MV}$ .

$$\epsilon_{MV} = P\left(\sum_{i=1}^m z_i - m\epsilon_\lambda \geq \frac{m}{2} - m\epsilon_\lambda\right) \quad (19)$$

$$\leq \exp\left(\frac{-2\left(\frac{m}{2} - m\epsilon_\lambda\right)^2}{m}\right) \quad (20)$$

$$= \exp\left(-2m\left(\frac{1}{2} - \epsilon_\lambda\right)^2\right). \quad (21)$$

Next, we plug the bound from (21) into (18) to obtain the following expression for  $\|C_{\epsilon_{MV}}^{-1}\|_\infty$ .

$$\|C_{\epsilon_{MV}}^{-1}\|_\infty = (1 - 2\epsilon_{MV})^{-1} \quad (22)$$

$$\leq \left(1 - 2\exp\left(-2m\left(\frac{1}{2} - \epsilon_\lambda\right)^2\right)\right)^{-1}. \quad (23)$$

To complete the proof, we need the following to hold:  $\|C_{\epsilon_{MV}}^{-1}\|_\infty \leq \|C_{\epsilon_\lambda}^{-1}\|_\infty$ , but due to the monotonicity of  $\|C_\epsilon^{-1}\|_\infty$ , it is sufficient to show that  $\epsilon_{MV} \leq \epsilon_\lambda$ .

Recall that  $\epsilon_{MV} \leq \exp\left(-2m\left(\frac{1}{2} - \epsilon_\lambda\right)^2\right)$ , so if we set  $\exp\left(-2m\left(\frac{1}{2} - \epsilon_\lambda\right)^2\right) \leq \epsilon_\lambda$ , we obtain the minimum number of label functions,  $m$ , required to ensure  $\epsilon_{MV} \leq \epsilon_\lambda$ .

$$\begin{aligned} \exp\left(-2m\left(\frac{1}{2}-\epsilon_\lambda\right)^2\right) &\leq \epsilon_\lambda \\ \Rightarrow m &\geq \frac{\log(1/\epsilon_\lambda)}{2\left(\frac{1}{2}-\epsilon_\lambda\right)^2}. \end{aligned}$$

Plugging (23) into Theorem 1, we obtain the following

$$\begin{aligned} d_{\text{TV}}(\tilde{P}_{\text{MV}}, \tilde{Q}_{\text{MV}}) &\leq d_{\text{TV}}(P, Q) \leq \|C_{\epsilon_{\text{MV}}}^{-1}\|_\infty d_{\text{TV}}(\tilde{P}_{\text{MV}}, \tilde{Q}_{\text{MV}}) \\ &\leq \left(1 - 2\exp\left(-2m\left(\frac{1}{2}-\epsilon_\lambda\right)^2\right)\right)^{-1} d_{\text{TV}}(\tilde{P}_{\text{MV}}, \tilde{Q}_{\text{MV}}) \\ &\leq (1 - 2\epsilon_\lambda)^{-1} d_{\text{TV}}(\tilde{P}_{\text{MV}}, \tilde{Q}_{\text{MV}}) \\ &= \|C_{\epsilon_\lambda}^{-1}\|_\infty d_{\text{TV}}(\tilde{P}_{\text{MV}}, \tilde{Q}_{\text{MV}}) \end{aligned}$$

which completes the proof.  $\square$

Notice that the proof of Proposition 1 does not depend on total variation distance beyond the dependence on Theorem 1. As such, Proposition 1 can be stated more generally in terms of the Integral Probability Metric induced by the GAN discriminator  $\mathcal{F}$  using Theorem 2 of Thekumparampil et al. [61]:

$$d_{\mathcal{F}}(\tilde{P}_{\text{MV}}, \tilde{Q}_{\text{MV}}) \leq d_{\mathcal{F}}(P, Q) \leq \|C_{\epsilon_{\text{MV}}}^{-1}\|_\infty d_{\mathcal{F}}(\tilde{P}_{\text{MV}}, \tilde{Q}_{\text{MV}}) \leq \|C_{\epsilon_\lambda}^{-1}\|_\infty d_{\mathcal{F}}(\tilde{P}_{\text{MV}}, \tilde{Q}_{\text{MV}}).$$

Finally, notice that Proposition 1 is made in terms of  $d_{\mathcal{F}}(\tilde{P}_{\text{MV}}, \tilde{Q}_{\text{MV}})$  and not in terms of  $d_{\mathcal{F}}(\tilde{P}_\lambda, \tilde{Q}_\lambda)$ . We can show that as the number of LFs approach infinity, we recover the distance under the clean labels:  $d_{\mathcal{F}}(P, Q)$ . Applying Theorem 1 to majority vote and a single LF results in the following two expressions:

$$d_{\mathcal{F}}(\tilde{P}_{\text{MV}}, \tilde{Q}_{\text{MV}}) \leq d_{\mathcal{F}}(P, Q) \leq \|C_{\epsilon_{\text{MV}}}^{-1}\|_\infty d_{\mathcal{F}}(\tilde{P}_{\text{MV}}, \tilde{Q}_{\text{MV}}) \quad (24)$$

$$d_{\mathcal{F}}(\tilde{P}_\lambda, \tilde{Q}_\lambda) \leq d_{\mathcal{F}}(P, Q) \leq \|C_{\epsilon_\lambda}^{-1}\|_\infty d_{\mathcal{F}}(\tilde{P}_\lambda, \tilde{Q}_\lambda) \quad (25)$$

Rearranging terms, we obtain the following

$$1 \leq \frac{d_{\mathcal{F}}(P, Q)}{d_{\mathcal{F}}(\tilde{P}_{\text{MV}}, \tilde{Q}_{\text{MV}})} \leq \|C_{\epsilon_{\text{MV}}}^{-1}\|_\infty \leq \|C_{\epsilon_\lambda}^{-1}\|_\infty$$

and

$$1 \leq \frac{d_{\mathcal{F}}(P, Q)}{d_{\mathcal{F}}(\tilde{P}_\lambda, \tilde{Q}_\lambda)} \leq \|C_{\epsilon_\lambda}^{-1}\|_\infty.$$

Notice that  $\|C_{\epsilon_\lambda}^{-1}\|_\infty$  has no dependence on  $m$  since it's a single LF, but  $\|C_{\epsilon_{\text{MV}}}^{-1}\|_\infty$  approaches 1 as  $m \rightarrow \infty$ :

$$\begin{aligned} \lim_{m \rightarrow \infty} 1 &\leq \frac{d_{\mathcal{F}}(P, Q)}{d_{\mathcal{F}}(\tilde{P}_{\text{MV}}, \tilde{Q}_{\text{MV}})} \leq \|C_{\epsilon_{\text{MV}}}^{-1}\|_\infty \leq \|C_{\epsilon_\lambda}^{-1}\|_\infty \\ \Rightarrow 1 &\leq \frac{d_{\mathcal{F}}(P, Q)}{d_{\mathcal{F}}(\tilde{P}_{\text{MV}}, \tilde{Q}_{\text{MV}})} \leq 1 \leq \|C_{\epsilon_\lambda}^{-1}\|_\infty \\ \Rightarrow d_{\mathcal{F}}(P, Q) &= d_{\mathcal{F}}(\tilde{P}_{\text{MV}}, \tilde{Q}_{\text{MV}}). \end{aligned}$$

Hence we obtain a stronger bound as the number of LFs increases.

### **F.3 Extensions**

For the sake of clarity, we make several simplifying assumptions in Claims (1) and (2). Both claims use the simplest possible aggregation strategy for weak supervision—majority vote, and our analysis in Claim (1) involves the use of a Gaussian mixture model—a less complex object of study compared to a GAN. We can directly extend both analyses to use more sophisticated weak supervision label models instead of majority vote, and different generative models, which should lead to improved bounds at the expense of a more complex claim statement. We note, additionally, that neither of the claims attempt to provide deep insight into the benefits of *jointly* learning the generative model and the label model—but this can be done with a slightly more careful analysis.